Time Resolved Transient Absorption Spectroscopy of Rhodamine 6G in Ethanol

Development and validation of a transient absorption spectroscopy setup for measurements on organic molecular crystals with femtosecond temporal resolution

by

Peter Antonius Aldegonda Dullens

Fontys University of Applied Sciences,
Applied Physics
&
Max Planck Institute
for the Structure and Dynamics of Matter

Fontys
University of Applied Sciences

mpsd
Max-Planck-Institut für
Struktur und Dynamik der Materie

Time Resolved Transient Absorption Spectroscopy of Rhodamine 6G in Ethanol

Author
Peter Antonius Aldegonda Dullens
p.dullens@student.fontys.nl
p.a.a.dullens@gmail.com
+31 6 36527697

University
Fontys University of Applied Sciences
Applied Physics
Rondom 1, 5612 AP
Eindhoven, The Netherlands

Academic mentor
Dr. Albert Bart Smit
ab.smit@fontys.n
+31 6 82094357

Period
4 September 2023 - 8 February 2024

Date of Submission
29 January 2024

Institute
Max Planck Institute
for the Structure and Dynamics of Matter
Scientific Support Unit Ultrafast Beams
Notkestraße 85, 22607
Hamburg, Germany

Institute mentor
Dr. Heinrich Schwoerer
heinrich.schwoerer@mpsd.mpg.de
+49 40 8998 88281

Approved: _____
Hamburg, 29 January 2024

Summary

At the Max Planck Institute for the structure and dynamics of matter, within the scientific support unit ultra fast beams research is ongoing on organic crystals using a setup which combines Femtosecond Transient Absorption Spectroscopy (TAS) and Ultrafast Electron Diffraction (UED). These two experiments respectively unravel information about the spectroscopic and structural behavior of these solids in their excited states. The research discussed in this report focuses on the development and characterisation of this TAS setup and the first TAS measurements on rhodamine 6G dissolved in ethanol to validate the setup.

Using TAS the difference in absorption between excited and ground states of a sample is measured. For the positive changes excited state absorption is the physical underlying process and for negative changes stimulated emission. Besides stimulated emission bleach can also cause a negative change, this signal is dependent on the excitation wavelength and relates to the population of the excited state.

The TAS setup uses to measure these signals consist of two different laser beams with each their own properties. Both of these beams originate from the same laser light source which generates laser pulses which last about 50 fs. The first beam is called the probe beam and serves the purpose of a light source analogous to one used with static absorption spectroscopy. The other beam which is called the pump beam is used to excite the sample to see the dynamics of the excited states. To calculate a change in absorption caused by exciting the sample two types of spectra are needed. The first spectrum will serve as a reference spectrum of the ground state while the second contains the signal of the excited state which is of interest. These excited state spectra also depend on the delay between the arrival of the pump and the probe beam at the sample. For this reason the setup is build so the path length and thus the arrival of the pump beam can be varied.

The probe beam needs to have a broad spectrum in the range which TAS measurements are taken and still needs to have a short pulse length in the femtosecond range. To achieve this a process called White-Light Generation (WLG) is used, which originates from an a number of non-linear processes when high intensity light is focused in a bulk transparent medium. The pump beam is used to excite the sample which the TAS measurement is taken of. Therefore its wavelength needs to be adjusted to an absorption wavelength of the sample, but its length still needs to stay short. This is done by using Noncollinear Optical Parametric Amplification (NOPA) with two amplification stages, followed by a prism compressor. After this a delay stage is implemented to vary the path length and an optical chopper is used to block the pump beam for half of the measurements, so only the probe beam is present in these. This last part is needed to get spectra of the sample in its ground- and excited state.

The first TAS measurement which have been executed were of the coherent artifact in pure ethanol. Through these measurements the delay at which the pump and probe beam overlap is found, this point is called time zero. This artifact which is seen in liquids also holds information about the chirp in the resulting spectra and the temporal resolution of the setup. Chirp is the difference in time of arrival between different wavelengths due to dispersion. From the measured results the curvature of this chirp has been determined to be equal to the function: $\Delta t_{chirp} = -1,24 \cdot 10^{-05} \cdot \lambda^2 + 5,37^{-02} \cdot \lambda - 5,37$. Besides this the maximal temporal resolution of the developed TAS setup has been determined to be around 180 fs.

After this measurements on rhodamine 6G dissolved in ethanol have been done. The first measurement of rhodamine 6G was done around time zero, to check the difference between the signal before and after this point and get the strongest possible signal. In the results of this a excited state absorption signal can be seen around 450 nm and a very strong bleach signal at 530 nm are observed. To map the temporal evolution of these two signals a longer delay range has been measured, which spanned to the maximal reachable delay by the setup of 2 ns. In these measurements it can be observed that these two signals both decay exponentially at first, but after that decay through a slower process which could not be identified in the current range of the setup takes over. By applying an exponential fit to the decay till 180 ps a initial decay constant 18,8 ps of has been found for the bleach signal around 530 nm and a initial decay constant 47,9 ps for the excited state absorption signal around 450 nm.

From these results can be concluded that: the chirp inherent to the setup is now known and can be corrected for, that the maximum temporal resolution of the setup is equal to 180 fs and that the results from measurements on rhodamine 6G prove the setup is valid.

This validation of the developed setup opens the door for further research on more complex organic crystals. Besides this the integration of a copy of this setup in a vacuum chamber were samples can be cooled to 10 K will be the next step of this project. This is the same setup integrating TAS and UED together, which has been mentioned before. There are also improvements to be be made in the setup in regards to the actual correction of the chirp, the temporal resolution and the processing of the results afterwards.

Samenvatting

Bij het Max Planck Institute for the Structure and Dynamics of Matter wordt binnen de Scientific Support Unit Ultra Fast Beams wordt onderzoek uitgevoerd naar organische kristallen met behulp van een opstelling die Femtoseconde Transient Absorption Spectroscopy (TAS) en Ultrafast Electron Diffraction (UED) combineert. Deze twee experimenten onthullen respectievelijk informatie over het spectroscopisch en structureel gedrag van deze vaste stoffen in hun geëxciteerde toestanden. Het onderzoek dat in dit verslag wordt besproken, richt zich op de ontwikkeling en karakterisering van deze TAS-opstelling en de eerste TAS-metingen op rhodamine 6G opgelost in ethanol om de opstelling te valideren.

Met behulp van TAS wordt het verschil in absorptie tussen geëxciteerde en grondtoestanden van een monster gemeten. Voor positieve veranderingen is geëxciteerde toestand absorptie het fysische onderliggende proces, en voor negatieve veranderingen gestimuleerde emissie. Naast gestimuleerde emissie kan bleach ook een negatieve verandering veroorzaken; dit signaal is afhankelijk van de excitatiegolflengte en heeft betrekking op de populatie van de geëxciteerde toestand.

De TAS-opstelling die wordt gebruikt om deze signalen te meten, bestaat uit twee verschillende laserbundels met elk hun eigen eigenschappen. Beide bundels komen uit dezelfde laserlichtbron die laserpulsen genereert die ongeveer 50 fs duren. De eerste bundel wordt de probebundel genoemd en dient als een lichtbron analoog aan een die wordt gebruikt bij statische absorptiespectroscopie. De andere bundel, die de pumpbundel wordt genoemd, wordt gebruikt om het monster te exciteren om de dynamiek van de geëxciteerde toestanden te observeren. Om een verandering in absorptie als gevolg van het exciteren van het monster te berekenen, zijn twee soorten spectra nodig. Het eerste spectrum dient als referentiespectrum van de grondtoestand, terwijl het tweede het signaal van de geëxciteerde toestand bevat dat van belang is. Deze geëxciteerde toestandspectra zijn ook afhankelijk van het tijdsverschil tussen de aankomst van de pump- en probebundel bij het monster. Daarom is de opstelling zo gebouwd dat de lengte van het pad van de pumpbundel en dus de aankomst kan worden gevarieerd.

De probebundel moet een breed spectrum hebben in het bereik waarin TAS-metingen worden uitgevoerd en moet toch een korte pulsduur behouden in het femtoseconde-bereik. Om dit te bereiken wordt een proces genaamd White-Light Generation (WLG) gebruikt, dat voortkomt uit een aantal non-lineaire processen wanneer intens laserlicht wordt gefocust in een bulk transparant medium. De pumpbundel wordt gebruikt om het monster te exciteren waarvan de TAS-meting wordt uitgevoerd. Daarom moet de golflengte ervan worden aangepast aan de absorptiegolflengte van het monster, maar de lengte van de puls moet kort blijven. Dit wordt gedaan door Noncollinear Optical Parametric Amplification (NOPA) te gebruiken met twee versterkingsfasen, gevolgd door een prisma-compressor. Daarna wordt een vertragingstrap geïmplementeerd om de padlengte te variëren, en een optische chopper wordt gebruikt om de pumpbundel voor de helft van de metingen te blokkeren, zodat alleen de probebundel aanwezig is. Dit laatste is nodig om spectra van het monster in zijn grond- en geëxciteerde toestand te verkrijgen.

De eerste TAS-metingen die zijn uitgevoerd, waren van het coherente artefact in ethanol. Met behulp van deze metingen is het tijdstip vastgesteld waarop de pump- en probebundel samenvallen; dit punt wordt tijd nul genoemd. Dit artefact dat wordt gezien in vloeistoffen bevat ook informatie over de 'chirp' in de resulterende spectra en de temporele resolutie van de opstelling. Chirp is het verschil in aankomsttijd tussen verschillende golflengtes als gevolg van dispersie. Uit de gemeten resultaten is de kromming van deze chirp bepaald als gelijk aan de functie: $\Delta t_{chirp} = -1,24 \cdot 10^{-05} \cdot \lambda^2 + 5,37^{-02} \cdot \lambda - 5,37$. Naast dit is de maximale temporele resolutie van de ontwikkelde TAS-opstelling bepaald op ongeveer 180 fs.

Hierna zijn metingen gedaan op rhodamine 6G opgelost in ethanol. De eerste meting van rhodamine 6G zijn rond tijd nul uitgevoerd, om het verschil tussen het signaal vóór en na dit punt te controleren en het sterkst mogelijke signaal te verkrijgen. In de resultaten van dit onderzoek is al een geëxciteerd toestand absorptiesignaal te zien rond 450 nm en een zeer sterk bleachsignaal rond 530 nm. Om de temporele evolutie van deze twee signalen in kaart te brengen, is een langer bereik gemeten, die reikte tot de maximale bereikbare vertragingstijd van de opstelling van 2 ns. In deze metingen is te zien dat deze twee signalen beide aanvankelijk exponentieel afnemen, maar daarna volgens een langzamer proces afnemen dat niet kon worden geïdentificeerd in het huidige bereik van de opstelling. Door een exponentiële fit toe te passen op het verval tot 180 ps, is een initiële vervalconstante van 18,8 ps gevonden voor het bleachsignaal op 530 nm en een initiële vervalconstante van 47,9 ps voor het geëxciteerde toestandsabsorptiesignaal op 450 nm.

Uit deze resultaten kan worden geconcludeerd dat: de inherent aan de opstelling verbonden chirp nu bekend is en gecorrigeerd kan worden, dat de maximale temporele resolutie van de opstelling gelijk is aan 180 fs en dat de resultaten van metingen op rhodamine 6G aantonen dat de opstelling geldig is.

Deze validatie van de ontwikkelde opstelling opent de deur voor verder onderzoek naar complexere organische kristallen. Naast dit zal de integratie van een kopie van deze opstelling in een vacuümkamer waar monsters tot 10 K kunnen worden gekoeld, de volgende stap zijn in dit project. Dit is dezelfde opstelling waarbij TAS en UED samen worden geïntegreerd, zoals eerder vermeld. Er zijn ook verbeteringen mogelijk in de opstelling met betrekking tot de daadwerkelijke correctie van de chirp, de temporele resolutie en de verwerking van de resultaten achteraf.

Preface

This report in front of you has been written as a part of an internship for my Bachelor's degree in Applied Physics at Fontys University of Applied Sciences in Eindhoven. The internship was executed at the Max Planck Institute for the Structure and Dynamics of Matter in Hamburg, specificly within the Scientific Support Unit Ultrafast Beams. This internship took place in the period from 4 September 2023 until 8 February 2024.

First of all I want to say that could not have wished for a greater experience for my internship in Hamburg. I am most grateful for everything I got to learn and all the incredible people I got to work with and meet during this time. Especially, I want to thank Dr. Heinrich Schwoerer and Dr. Gabriele Tauscher for making me feel at home at the institute directly from the start of my internship. I could not have imagined more kind and welcoming people to work with. Besides that I also want to thank Michiel Jansen for telling me about his great experience at the institute, which got me interested in the work that I got to be part of. I also want to thank Dr. Bart Smit for getting me in touch with the people at the institute and his continuous interest in my progress.

The research presented in this report would not have been possible without the contribution of a number of people, whom I would like to thank for this. First of all, I would like to thank Dr. Heinrich Schwoerer and Dr. Gabriele Tauscher for guiding me in my research and transferring their knowledge to me. They were always happy to help and to get the most out of the research described in this report. Besides This I want to thank Dr. Bart Smit as my academic mentor during this project and for all the feedback he gave me. I also want to thank Dr. Sascha Epp for his contribution to the integration of the camera control software into the sever infrastructure in the lab. Besides that I want to thank all the other employees of the Max Planck institute for the Structure and Dynamics of Matter who in some way contributed to this project, you were always helpful and a pleasure to work with. It was an honour and a real pleasure for me to work on this project with all of you.

Thank you all - Vielen Dank an alle

Sincerely,

Peter Antonius Aldegonda Dullens

Hamburg, 25 January 2024

Terminology

The terminology contains all the abbreviations and symbols from the Latin and Greek alphabet used in this report, these three categories are all grouped independent of each other. All these categories are independently sorted in alphabetical order.

Abbreviations

AC Alternating Current
BBO Barium Borate
DC Direct Current
GDD Group-Delay Dispersion
GVD Group-Velocity Dispersion
ND Neutral Density
NOPA Noncollinear Optical Parametric Amplification
OLED Organic Light Emitting Diode
OPA Optical Parametric Amplification
SHG Second Harmonic Generation
SPM Self-Phase Modulation
TAS Transient Absorption Spectroscopy
UED Ultrafast Electron Diffraction
WLG White-Light Generation

Latin symbols

A Absorbance of a material [−]
C Concentration of a species in solution $[\frac{mol}{m^3}]$
c Speed of light equal to 299.792.458 $[\frac{m}{s}]$
e Euler's number equal to 2.718 [−]
I Intensity of a light beam $[\frac{W}{m^2}]$
$\mathbf{I_0}$ Intensity of the incident or unpumped light $[\frac{W}{m^2}]$
$\mathbf{I_a}$ Intensity of the reference light $[\frac{W}{m^2}]$
$\mathbf{I_b}$ Intensity of the signal light $[\frac{W}{m^2}]$
$\mathbf{I}^*$ Intensity of the pumped light $[\frac{W}{m^2}]$
i Complex number arising from $i^2 = -1$ [−]
l Optical path length $[m]$
n Refractive index of a material [−]
$\mathbf{n_k}$ Nonlinear refractive index for a material $[\frac{m^2}{W}]$
$\mathbf{S}(\mathbf{t})$ Electric field of a laser pulse $[\frac{V}{m}]$
$\mathbf{S}(\omega)$ Spectrum of a laser pulse $[a.u.]$
t Time $[s]$
v Speed of light in a dielectric medium $[\frac{m}{s}]$

Greek symbols

α Variable for an angle $[rad]$
β Variable for an angle $[rad]$
ΔmOD Change in optical density times 10^3 [−]
Δn Change in refractive index by the Kerr effect [−]
ΔOD Change in optical density [−]
Δt Delay to a reference value $[ps]$
Δt_{chirp} Shift in delay due to chirp $[ps]$
$\Delta\omega$ Spectral width of a laser pulse $[m]$
λ Wavelength of light $[m]$ or nm
ξ Absorption of species $[\frac{m^2}{mol}]$
π Mathematical constant equal to 3.14 [−]
τ Pulse width $[s]$
ϕ Phase of a electric wave $[rad]$
ω Angular frequency of an electric wave $[\frac{rad}{s}]$

Contents

List of Figures

List of Tables

1 Introduction

Molecular solids have many interesting properties that bring together their abundance of spectroscopic processes in organic molecules with the electrical properties of condensed matter. These fascinating solids already found their way into applications such as the Organic Light Emitting Diode (OLED) and the photovoltaic cell, which are widely used today. The microscopic interaction of the electronic molecular orbitals with light and the distant propagation of charges and energy within the crystal are the two fundamental physical processes which govern all electro-optical applications of organic solids. Getting insight into these processes can result in a deeper understanding of the properties of a given solid and how they may be improved to better suit a specific use case.

One of the ways to research these molecular solids, which this project focuses on, is through spectroscopy. At its most basic form this is done through static absorption spectroscopy, which reflects the energy differences between occupied and unoccupied electronic states and shows possible electronic excitation channels. When these channels are known it opens the way to controlled photoinduced experiments, like absorption spectroscopy of exited states. Other than static absorption spectroscopy, the absorption spectroscopy of exited states has a temporal evolution that contains useful information about the processes at play. To track this temporal evolution femtosecond Transient Absorption Spectroscopy (TAS) is used, where snapshots of absorption spectra of the crystals are taken at defined times after excitation. This femtosecond TAS is the main focus of this study on rhodamine 6G in solution.

The TAS setup which is developed and validated during this project will be part of a larger setup in which TAS and Ultrafast Electron Diffraction (UED) are combined to take both measurements of an sample after each other. For this combined setup the samples are situated in a vacuum chamber at high vacuum and can be cooled to temperature of approximately 10 K. When this setup eventually is fully working it can efficiently measure TAS spectra to investigate the electronic properties of a molecule and after that UED images can be taken to measure the change in structure, both at low temperatures and in vacuum. In this report only TAS is considered, so a understanding of UED is not needed. But these UED experiments are still relevant in the context of the whole setup which combines TAS and UED.

In this report the main focus is the time resolved transient absorption behavior of rhodamine 6G in ethanol. These measurements are in itself nothing new and are well documented in literature. For this reason this sample has been chosen to be the first sample analysed using the new TAS. This is done since the final goal of this project is to characterise the behavior of the setup and validate it is working correctly. By doing this the setup is being prepared for research on less documented samples in the future. The research question of this report can therefore be phrased as: *What are the experimental parameters and their limitations of the TAS setup developed during this project and what do measurements of rhodamine 6G dissolved in ethanol show in terms of the validity of the results of the current setup?* This research question can be further divided into some subquestion which are as follows:

- What is the temporal resolution in the measured transient absorption spectra from the setup?
- What is the wavelength dependence of the temporal evolution (chirp) induced into the measured transient absorption spectra from the setup?
- What do measurements on rhodamine 6G dissolved in ethanol show in terms of validity of the setup?

Although the main focus of this report is the spectroscopic research on rhodamine 6G, a big part of this project has also been the development of control software for detectors, experimental control software and building the setup which is used to get the results in this report. For this reason this report also contains a in depth description of the setup and methods. Therefore the results are considered in a more general sense in terms of the underlying physical processes. This can be justified by the extensive literature about both the samples and the optical processes they give rise to.

The report before you is structured in the following way: In chapter 2 the theoretical background needed to understand the setup, methodology and results is explained. The methodology of the experiments is explained in chapter 3. The results from the executed experiments are considered in chapter 4 after which their uncertainties and accuracy are discussed in chapter 5. The conclusion of the experiments is presented in chapter 6 followed by the outlook of the conducted research in chapter 7.

2 Theory

The following chapter is divided into three sections, which are: Linear optical phenomena, Nonlinear optical phenomena and Interaction of light with molecules. The theory in these sections contributes to understanding the project as a whole. Each section will start with a short introduction explaining their relevance to the project this report describes.

2.1 Linear optical phenomena

In this section Attenuation, Ultra short pulses and Dispersion will be considered. These phenomena are essential in the functioning of the setup and are also useful to understand the results which will arise from it.

2.1.1 Absorption

Transient Absorption Spectroscopy (TAS) is a measurement method which is directly connected to the absorption of light, as the name already suggests. Absorption or optical density is known as the partial loss of intensity of a beam traveling through a dielectric medium. This property depends on the wavelength of light and is specific to a material.

The Beer-Lambert law also known as Beer's law relates the absorbance and concentration of a substance at a fixed wavelength to each other. This law states that the intensity of radiation and amount of optically active matter is linearly correlated. Although at first this law was stated as an empirical law, the modern form is formulated in a more general mathematical form. The most common expression for Beer's law is shown in equation 2.1. This form of Beer's law is generally used when the attenuating species is suspended in a transparent liquid. I is the intensity after passing the sample in $\frac{W}{m^2}$, I_0 is the intensity of the incoming light in $\frac{W}{m^2}$, A is the absorbance or optical density, ξ the absorptivity of the attenuating species in $\frac{m^2}{mol}$, l the optical path length through the medium in m and C the concentration of the attenuating species in $\frac{mol}{m^3}$.[1]

$$\log\left(\frac{I_0}{I}\right) = A = \xi l C \tag{2.1}$$

The attenuation of a material can also be defined in other forms. For these definitions l and A will be the same but the units of ξ and C will change to for example $\frac{1}{m^3}$ and m^2 for crystals. This is connected to the way of measuring concentration or density and absorption in regards to this, but is not really relevant to describe further for now.

With TAS measurements the only interest lies in measuring the difference in absorption between two situations. In this case it is possible to only measure the transmitted light after the absorbing medium. This results in a simpler setup. The equation for calculating this difference in absorption is shown in equation 2.2. In this equation ΔOD is the difference in absorption, I_b the intensity of the state used as a reference, I_a^* the intensity of the new state to compare.

$$\Delta OD = -log\left(\frac{I_a^*}{I_b}\right) \tag{2.2}$$

2.1.2 Ultra short pulses

The base of the research discussed in this report is a laser light source which produces ultrashort laser pulses at high intensities. The laser produces single laser pulses which have a duration of less than 50 femtoseconds. When looking at the spectral properties of these ultra-fast pulses, it can be seen that their spectra are relatively wide. To understand why this happens the mathematical method of Fourier transformation is needed. In Appendix A an overview of the Fourier transform is given together with the Fourier transform of a Gaussian.

Before analyzing laser pulses a mathematical description of such a pulse is needed. A good way to describe an electric wave is by using a cosine function with a specific wavelength and phase, but in this case the pulse is not limited in time. To do this the function can be multiplied by a Gaussian function, this creates a cosine function contained in a Gaussian. How the electric field of such a pulse looks is shown in figure 2.1a. The mathematical function for this pulse is shown in equation 2.3. This description of a wave in a Gaussian envelope is known to be a good model for a laser pulse. The electric wave has a angular frequency $\omega = c/\lambda$ in which c is the speed of light and λ is the wavelength. Besides that it has a duration equal to 2τ and a phase determined by ϕ.

$$S(t) = e^{-\frac{t^2}{\tau^2}} \cdot \cos(\omega_0 t - \phi) \tag{2.3}$$

By inserting equation 2.3 into the Fourier transformation in equation A.5 and solving this the Fourier transform $S(\omega)$ can be found. To solve this the identity $\cos(\alpha)\cdot\cos(\beta) = \frac{1}{2}(\cos(\alpha-\beta)+\cos(\alpha+\beta))$ and the definite integral

$\int_0^\infty e^{-a^2x^2} \cdot \cos(bx)dx = \frac{\sqrt{\pi}}{2a} \cdot e^{-\frac{b^2}{4a^2}}, a > 0$ are needed. The Fourier transform can be found as follows:

$$\begin{aligned} S(\omega) &= \int_{-\infty}^{\infty} e^{i2\pi\omega t} \cdot e^{-\frac{t^2}{\tau^2}} \cdot \cos(\omega_0 t - \phi)dt \\ &= \int_0^{\infty} e^{-\frac{t^2}{\tau^2}} \cdot \cos(\omega - \omega_0)t \cdot dt + \int_0^{\infty} e^{-\frac{t^2}{\tau^2}} \cdot \cos(\omega - \omega_0)t \cdot dt \\ &= \frac{\tau\sqrt{\pi}}{2}\left(e^{-(\omega-\omega_0)^2(\frac{\tau}{2})^2} + e^{-(\omega+\omega_0)^2(\frac{\tau}{2})^2}\right) \\ S(\omega) &= \frac{\tau\sqrt{\pi}}{2} \cdot e^{-(\omega-\omega_0)^2(\frac{\tau}{2})^2} \end{aligned} \tag{2.4}$$

The result from this Fourier transformation shown in equation 2.4 is a Gaussian curve. In figure 2.1b the resulting curve for the Fourier transform can be seen. The $1/e$ duration of the pulse has a duration of τ and the spectral width is is equal to $\Delta\omega = 2/\tau$. The dependence of the spectral width on the temporal width gives a limit for the spectral width of a pulse or vise versa. In practice this means that ultra-short pulses have a broad spectrum and that to achieve a narrow spectrum a long pulse is needed. Light pulses which reach this limit are called Fourier-transform-limited pulses or bandwidth-limited pulses. In most practical cases the limits are not reached, but some rough approximations and comparison between these pulses proves to be useful. For example most laser pulses which are discussed in this report have temporal pulse widths double that of the Fourier-transform-limited pulses.[2]

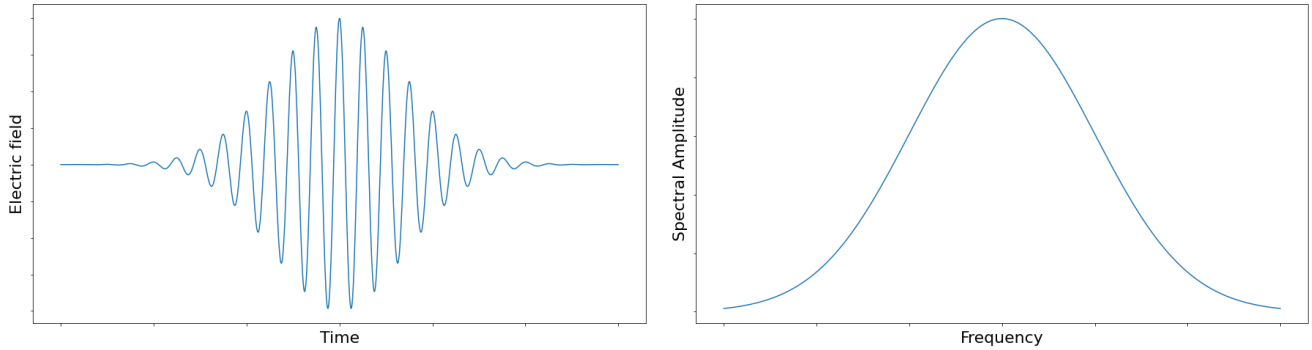

(a) Electric field of a laser pulse constrained by a Gaussian envelope.

(b) Fourier transform of a Gaussian pulse, which results in the spectrum.

Figure 2.1: Both the electric field of a Gaussian pulse and the spectrum from such a pulse.

2.1.3 Dispersion

When travelling through a vacuum all electromagnetic waves have the same speed. This speed of 299.792.458 $\frac{m}{s}$ with the symbol c is a fundamental constant which is crucial to much of the known physics today. When traveling through other dielectric media this speed is dependent on the wavelength and the specific material. In optics the property describing this is the refractive index, which relates the speed of light in a specific medium to the speed of light in a vacuum. In equation 2.5 this shown with n being the refractive index, c the speed of light in vacuum and v the speed of light in the specific material.

$$n(\lambda) = \frac{c}{v(\lambda)} \tag{2.5}$$

This difference in speed which causes dispersion is well know in optics. It causes effects like spatially dividing different colors of light in prisms and rainbows, which most people are familiar with. With ultrashort pulses dispersion also comes in to play. Dispersion in short pulses causes them to broaden in temporal width. This originates from the difference in speed between the fastest and the slowest wavelengths, and because of this difference, the pulse broadens over time. For this reason broadband pulses generally are longer than pulses with a narrow band. If the spectrum of such a broadband pulse could be measured when travelling through it, you would see the shorter wavelengths at the leading edge and the higher wavelengths at the falling edge. This kind of signal that you would observe over time is called a chirp. When taking measurements of light it should be considered that due to chirp higher wavelengths will arrive later at a sample or detector than shorter wavelengths. This behavior of the chirp seems to contradict the relation between the behavior of short pulses as seen in the preceding subsection. The difference between these two relations is that the chirp can be corrected for to theoretically reach

the duration of a Fourier-transform-limited. How this can corrected for to compress pulses is later shown in the methodology in the next chapter.

The amount of chirp in a signal depends on the amount of material the light travels trough, the material and the bandwidth of the light. A quantity of how much chirp is generated in a material is the Group-Velocity Dispersion (GVD). With the GVD and the path length of the light through the material the chirp can be calculated. For simple systems this can be useful, but with more complex systems this becomes unpractical. In these cases it is better to just measure the chirp or pulse length.

Till now only chirp due to transmission has been considered, but some layered mirrors can also induce chirp. This chirp can not be defined by the GVD, so another quantity is needed to describe it. The Group-Delay Dispersion (GDD) is a related yet independent quantity which describes the chirp generated by layered mirrors. In regards to a practical setup it is optimal to use components with a GVD or GDD as low as possible when working with short pulses. This will keep the pulses short and minimizes the chirp in the end signal.

2.2 Nonlinear optical phenomena

The setup to create the two beams which will be discussed later in the methodology would not be possible without nonlinear optics. For the generation of ultrashort pulses with a broad spectrum the Kerr effect plays a big role. Therefore this effect and how it results in broadband laser pulses is considered here. Besides this nonlinear wave mixing processes play a big role in manipulating the spectra of more narrow banded pulses. Therefore in this section these processes are also considered in detail. This will result in a solid foundation for understanding the optical setup which will be discussed in the methodology.

In general nonlinear optics is understood as the domain of optics in which polarization density responds non-linearly to the electric field. This nonlinear behavior is typically observed with light at very high intensities at which the electric fields are comparable to the atomic electric fields. The processes which are relevant for this report can roughly be divided in two categories: phenomena originating from Frequency-mixing processes and phenomena resulting from an intensity-dependent refractive index. Which of these processes are observed in a said material are depending on the non-linearity and symmetry of the optical medium. First the origin and results of a intensity-dependent refractive index are considered. Following this Frequency-mixing processes are discussed alongside some of their applications.

2.2.1 Kerr effect

The Kerr effect is responsible for a change in refractive index proportional to the square of the electric field. This effect can be caused by an external Direct Current (DC) electric field or by the Alternating Current (AC) electric field of the light itself. For the purposes considered in this report only the latter is relevant, since the nonlinear optic which are used are all passive. The difference between the linear refractive index and the actual one when the AC Kerr effect is taken into account is shown in equation 2.6. In this equation Δn is the difference from the linear refractive index, n_k the nonlinear refractive index, and I the optical intensity. n_k depends on the material which explains why some material show more nonlinear behavior than others. For most transparent materials the value of n_k is in the order of 10^{-20} $\frac{m^2}{W}$, this explains why this effect only becomes relevant at high intensities.

$$\Delta n = n_k \cdot I \tag{2.6}$$

The main way of achieving high enough intensities to have a significant change in refractive index due to the AC Kerr effect is by using lasers. Their high power and relatively small beam size can result in a high intensity which can further be increased by focusing the beam. A property of most laser beams is that they follow a Gaussian intensity profile. This bell shape characteristic results in a focusing effect which arises from the gradient of refractive indexes due the AC Kerr effect. For this behavior to be significant the AC Kerr effect has to make a significant contribution to the refractive index. Resulting from this focusing effect laser beams can collapse into a channel of finite size when they reach a critical intensity which depends on the medium.

Another phenomenon resulting from the change in refractive index resulting from the AC Kerr effect is Self-Phase Modulation (SPM). This effect is only noticeable with ultrashort pulses. When one of these high intensity pulses travels through a medium it results in a varying refractive index, as a result from the Kerr effect. This change in refractive index will result in a change of the phase of the pulse and in term its spectrum. SPM for a Gausian pulse the leading edge of the pulse will end up with a higher wavelength and the trialling edge with a lower wavelength. The result of SPM is therefore the broadening of the spectrum of a pulse. Interestingly the process of SPM keeps the envelope or pulse width of the pulse unchanged. These characteristics are precisely the opposite of the dispersion induced by a positive GVD.

Solitons are optical fields which do not change while propagating. Most commonly these solitons are created by balancing the effects of dispersion with the non-linear effects caused by the Kerr effect. This is quite intuitive when considering that the SPM has the inverse properties in regards to a signal with a positive GVD. Solitons are considered here and of interest for this report, because they are directly linked to the non-linear process of

White-Light Generation (WLG). During this process a broadband spectrum is generated from a narrow band laser pulse. This spectrum is also often called a supercontinuum.[3][4][5]

The process which generates supercontinua is called soliton fission. Soliton fission takes place when a soliton becomes unstable and breaks down. During soliton fission higher order solitons break down into multiple fundamental solitons with small random variations. This in turn results in the supercontinua which are observed. For the scope of the execute research full understanding of soliton fission is not needed, but is useful to get an general idea of the processes the setup is based on. The practical setup to generate white light will be considered in the methodology in subsection 3.1.2.[6]

2.2.2 Wave-mixing processes

When electromagnetic waves are considered in non-linear material such as birefringent crystals, wave mixing becomes possible. If the wave equation in a nonlinear material is solved it results in a term which can function as a driver for a oscillation. This can in turn mix or couple energy between different frequencies, most of the time this process is called wave mixing. The three possible wave mixing processes which arise from the non-linear wave equation are second-harmonic generation, sum-frequency generation and difference-frequency generation. In all these processes momentum and energy must be conserved, therefore the energy and momentum before and after the process must always balance out. These three processes will all be explained to get a understanding of the processes and their applications.

In nonlinear optics it is possible to create a beam with a frequency double that of an incoming beam using a birefringing crystal. This is done using a process called Second Harmonic Generation (SHG), which can be intuitively be explained as taking two incoming photons and merging these together in a photon with twice the amount of energy. The physical process involved here is more analogous to a driven oscillator, wherein two electromagnetic waves amplify each other. For this to occur the phase of the incoming beam must carefully be matched to the birefringing crystal. The process of SHG is mostly used to double the frequency of laser light in optical setups, but also has another relevant application which will be discussed. In figure 2.2 a schematic overview of this process can be seen along side with the photon energies of the involved photons in figure 2.2a. It needs to be noted that there are no physical energy levels in this process, since the process arises from wave mixing.

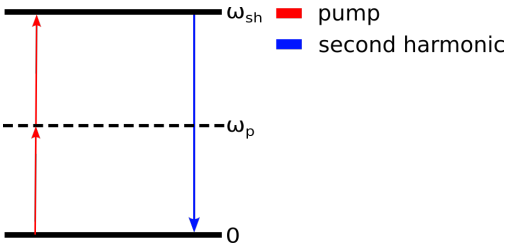

(a) Virtual energy levels for all the photons involved in the process of second harmonic generation.

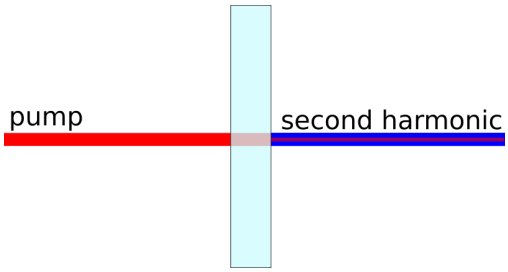

(b) Schematic view for the incoming and outgoing beams for second harmonic generation.

Figure 2.2: Overview of the energies of the photons involved in second harmonic generation and the beam directions for this process which relates to the conservation of momentum.

Another interesting fact which proves to be useful is that a SHG also can take place when two beams with identical wavelengths are sent through a nonlinear crystal. In figure 2.3 a schematic drawing is shown of the resulting beams of SHG for two incoming beams This results in the two single beams with the same direction as the incoming beams as seen before and a third beam precisely in between these two. For this third beam both beams generate a second harmonic together. This beam need to be in between the two other SHG beams since momentum must be conserved. An useful application of this is the measurement of the auto-correlation signal of a beam, since the middle beam is the result of the temporal overlap of two laser pulses. The intensity of this beam therefore is also depending on this overlap. In other words the third beam will only be visible if the beams overlap in the nonlinear crystal and its signal will be maximal if the pulses exactly arrive at the same time. How this auto correlation signal which can be measured using this process relates to the pulse width can be seen in Appendix A.1.

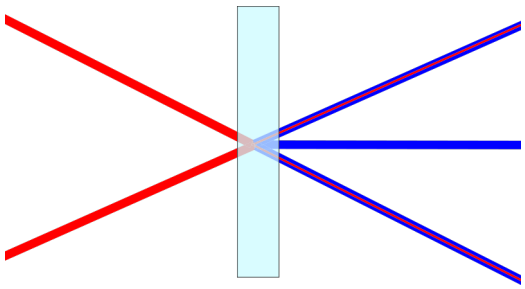

Figure 2.3: Schematic drawing of second harmonic generation for two incoming beams which overlap in a nonlinear crystal.

Optical Parametric Amplification (OPA) is a process in which a seed beam gets amplified using a pump beam, this results in a amplified seed beam, an idler beam and a residual beam from the pump beam. The physical process OPA relies on is difference-frequency generation and thus only takes place in nonlinear media. The four beams which are connected to this process are the incoming pump and seed beam and the outgoing amplified seed and idler beam. An overview of these beams and their direction can be seen in figure 2.4b

For OPA to work the pump beam needs to have a higher photon energy, than the seed beam. The reason for this is that the process takes a pump photon and generates an identical seed photon, because energy needs to be conserved another photon is created with a wavelength of the difference between the pump and the seed. This can be seen clearly in figure 2.4a which shows the energy of all the incoming and outgoing photons involved in the process. It needs to be noted that in this process there are no physical energy levels since it is an interaction between waves. These photons which have an energy equal to the difference in energy between the pump and the seed create the idler beam. For the photon momentum to be conserved this idler beams direction is on the other side of the pump beam as the seed. This can be seen in figure 2.4b.

The process of OPA is sensitive to the phase of the light waves involved. For this reason phase matching of the pump and seed beam is needed, to achieve a efficient conversion. The downside this gives rise to with OPA is that this phase matching can only be done for a specific wavelength. This makes OPA useful for amplifying laser beams of a static wavelength, but not suitable for amplifying a broad range of wavelengths.

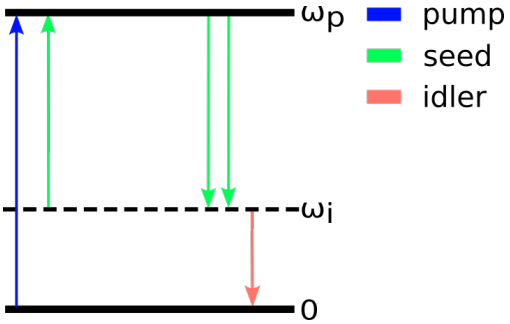

(a) Virtual energy levels for all the photons involved in the process of Optical parametric amplification.

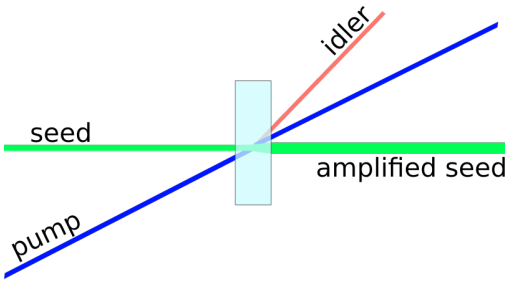

(b) Schematic view of the incoming and outgoing beams for Optical parametric amplification.

Figure 2.4: Overview of the energies of the photons involved in wave mixing and the beam directions for this process which relate to the conservation of momentum.

To achieve a higher efficiency for a broad wavelength range Noncollinear Optical Parametric Amplification (NOPA) can be used. This is based on the same process as OPA which is difference-frequency generation, but introduces critical phase matching. Due to this critical phase matching NOPA can be used across a broad spectral range at a high efficiency. This is done by creating a specific angle of the pump and the seed beam in regards to the optical axis of the crystal. Due to the non linearity of the birefringent crystal this results in constructive interference in a broad spectral range.

2.3 Interaction of light with molecules

Interaction of light with molecules is generally what is measured in TAS, therefore this plays a big role in the interpretation of the results. In this section the following Interaction of light with molecules are considered: Photo-excitation ant The dynamics of excited states. These interaction all are relevant to understanding the results which follow from TAS and are therefore considered here.

2.3.1 Photo-excitation

Photo-excitation of molecules is a well know phenomenon, it is what is measured using the traditional absorption spectroscopy most will be familiar with. Since it is still the basis for TAS and lays the foundation for the dynamics of excited states it is considered here.

To get a clear view of photo-excitation in molecules it is useful to first look at single atoms. First it is convenient to consider hydrogen which has only one electron. From solving the Schrödinger equation for a hydrogen atom its energy levels can be calculated for all its states. When this is done it shows that these energy levels are well defined and separated lines. If a photon with the exact amount of energy between two of these lines interacts with the atom, the electron can be excited to a higher energy state. Resulting from this only specific wavelengths of light are absorbed when broadband light is send through hydrogen atoms. In turn this results in the distinct spectral lines which is associated with hydrogen like atoms.

For molecules the structures that form them are a lot complexes, therefore the spectra are also less defined as in atoms. This is a result from the molecules consisting of multiple atoms and multiple free electrons, which creates more possible energy states. These states originate from vibrations in the molecular bonds or rotation of the molecule itself. The vibration states of a molecule are a lot closer together than the electronic states, and are independent of them. So every electronic state can be divided in vibrations sub states. This already gives the possibility for a lot more options for transitions and thus absorption. Besides this these vibrations states can again consist of rotational states, which are even more closer to each other. This again gives more options for transitions and thus absorption. For this reason the absorption of molecules is less defined than absorption in atoms. One property which is convenient is that the absorption spectra of molecules still have distinct maxima and minima. Therefore the absorption in molecules is often described in absorption peaks at a specific wavelength.

For convenience and to make it easy to visualise absorption and processes from this point on these complex systems will be simplified a bit. It is useful to describe optical interactions in terms of energy diagrams, which look at the energy of a single molecule. For absorption these energy diagrams will show a rise in energy, the amount of energy which is absorbed is dependent on the wavelength. To make the diagrams more clean these diagram use the wavelengths with a maximum in absorption. A energy diagram for a absorption is shown in figure 2.5.[7]

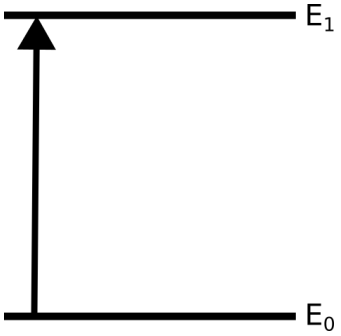

Figure 2.5: Energy diagram for absorption of a photon.

2.3.2 Dynamics of excited states

After photo-excitation a range of other processes can take place, these processes can be referred to as excited state dynamics. These dynamics are measured through the TAS measurements this report focuses on. The following processes will be considered here: excited state absorption, stimulated emission and bleach.

The first and most straightforward is excited state absorption. When a molecule is excited to a higher state it is possible to excite it again to an even higher state. The wavelengths where excited state absorption takes place can be different from absorption from the ground state, since the possible transitions are different at the excited state. An example for an energy diagram of excited state absorption is shown in figure 2.6a. The process of excited state absorption corresponds with an positive change in optical density in TAS measurements.

At an excited state there is also another process which can take place, which is stimulated emission. When stimulated emission takes place, a photon interacts with an excited molecule and stimulates the emission of another photon. This emitted photon is an identical copy of the photon stimulating it, meaning it has the same wavelength, phase and direction. In figure 2.6b an energy diagram for this process is shown. The process of stimulated emission corresponds to a negative change in optical density in TAS measurements, this is because more light exits the molecule than entering it. In some TAS measurements it is also possible for scattered light from a sample to cause a similar signal. This scattered light can be distinguished by the fact that it is there independent of the excitation of the molecule.

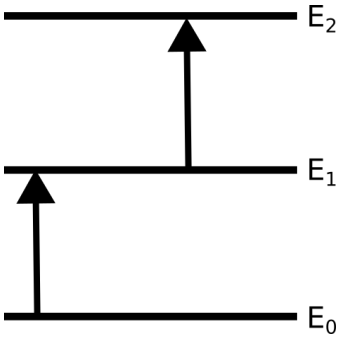

(a) Energy diagram for excited state absorption absorption of a photon.

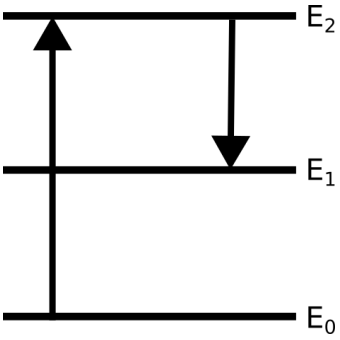

(b) Energy diagram for stimulated emission of an photon in an excited state.

Figure 2.6: Energy diagrams of absorption and emission in the excited states.

The last dynamic which will be considered is bleach. bleach originates from a molecule being excited to a state where further absorption is not possible. Because of this no more light can be absorbed in a specific region ,which results in a negative change in absorption. This signal originates from comparison between the ground state and an excited state in TAS measurements. Because of this a bleach signal is directly related to the population of the excited state. In some cases bleach can overshadow processes with a smaller signal, in this case bleach may be unwanted. Since bleach is directly connected to the excitation band, the sample can be excited in another region to move the bleach to another spectral region. in figure 2.7 a energy diagram for the process of bleach is shown.

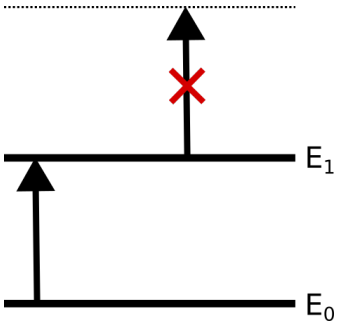

Figure 2.7: Energy diagram for bleach of an excited state.

3 Methodology

This chapter describes the Transient Absorption Spectroscopy (TAS) setup which has been developed and used during this project. Using this setup it is possible to measure transient absorption of samples with a temporal resolution of less than 100 fs. This is not a ordinary feat since this is the equivalent to the time it takes to travel the thickness of an human hair when traveling at the speed of light. How this achieved is first described in the following section about the optical setup. After this some thought is given to the acquisition and processing of these measurement since data is gathered at an rate of 1 kHz and the processing and handling of this data is nearly autonomous.

3.1 The optical setup

First it is useful to get an overview view of how TAS works. In contrast to the seemingly continuous graphs which result from TAS it is no continuous measurement over time. This makes sense since it is not possible to gather data from any sensor at a rate which yields a temporal resolution of around 100 fs. Therefore a pump-probe method is used to achieve this resolution, this means that instead of a continuous "movie" a TAS measurement consist of multiple "photos" at specific times. In the case of TAS first a sample is excited by an ultrashort pump laser pulse at an specific time, after which at a specific delay a ultrashort probe pulse probes the absorption of the sample. To measure the temporal evolution of an excited sample multiple measurements are done at a different delay from the arrival of the pump pulse. Using this method only every pulse needs to be measured before the next arrives after 1 ms, these measurement rates are relatively easy to reach. This makes it possible to measure at such a high temporal resolution, which is mainly limited by how long the laser pulses last. For the setup considered in this report the pump pulse width is about 50-70 fs and the probe pulse about 150 fs, this makes it possible to measure at such a high resolution using this setup. Varying the delay between these pulses with way higher accuracy's than the pulse lengths will later prove to be quite simple.

In figure 3.1 an overview of the complete setup used for TAS is shown. In the following subsections all parts of the setup which are shown in this figure will be considerd.

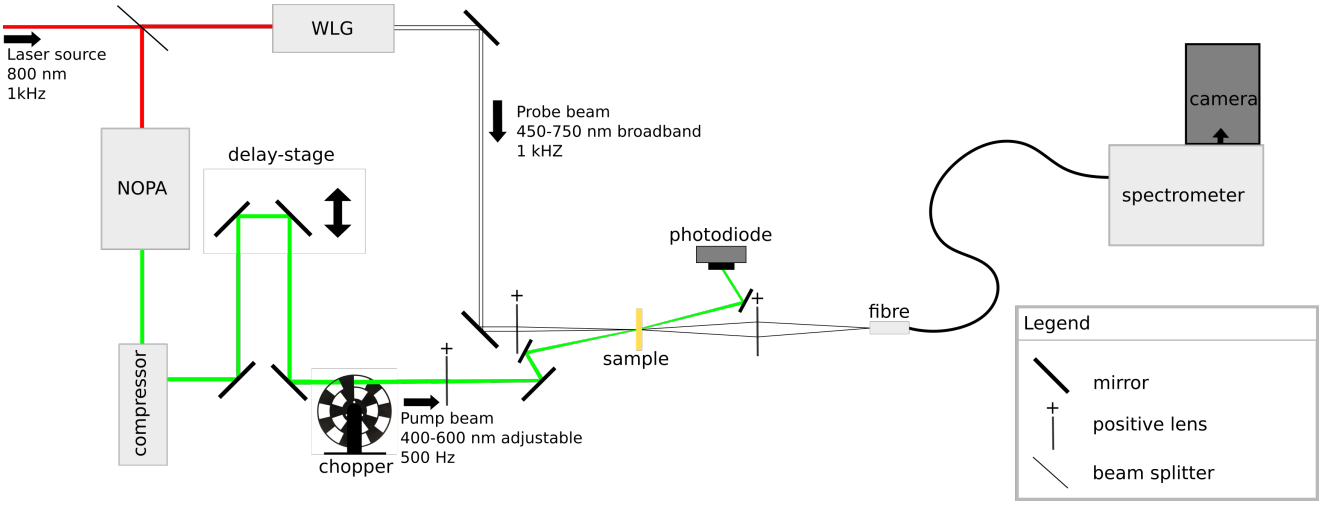

Figure 3.1: Schematic drawing of an overview of the whole TAS setup from source to the detector, the optical setup for white light generation(WLG), The Non-colinear amplification(NOPA), the pulse compressor and the spectrometer are shown as boxes to get a clean overview of the setup, the optical setup for these parts can be found in figures following this one.

3.1.1 Laser light source

The laser light entering the optical setup is generated by a amplified femtosecond Titanium:Sapphire laser. This laser generates pulse with widths below 50 fs. The centre wavelength of these pulses is 800 nm and the laser produces them at a rate of 1 kHz. From this 1 kHz repetition rate follows that this should also be the detection rate of the detectors used in the setup to catch each pulse. This alongside the high intensity produced by the source results in a range of non-linear processes, which are used throughout the optical setup. The laser produces light which is linearly polarized with horizontal orientation when exiting the laser. For convenience this direction of polarization is kept parallel to the optical table throughout the whole setup.

3.1.2 Probe beam

As can be seen in the overview in figure 3.1 the beam from the source is spilt into two paths by a beam splitter. These two beams are those of the probe (white) and the pump beam (green). The probe beam is used to take an absorption spectrum from the sample similar to static absorption spectroscopy. For this reason this spectrum should be broad and include all the wavelengths which are useful to measure for a chosen experiment. To get this kind of spectrum a White-Light Generation (WLG) setup is implemented in the probe beam. This part of the setup takes the laser light and transforms it into a broad and flat spectrum in the visible range. To achieve this the high intensity femtosecond pulses are focused in a bulk slab of sapphire, after which a supercontinuum is generated due to fission of created solitons. This process has already been described in subsection 2.2.1 of the theory. the generated supercontinuum is a broad and flat spectrum which is usable for the application of the probe beam. The spectrum of this supercontinuum varies depending on the material in which it is generated. Sapphire gives a spectrum in the visible range, but other material as for example calcium fluoride will result in a spectrum ranging from the UV to the visible range.

In figure 3.2 an optical setup is shown which can be used to generate white light. The components left from the sapphire window are used to vary some important parameters for the generation of white light, these will be discussed first. The first parameter which needs to be adjustable is the intensity of the incoming light. For the WLG process to take place an intensity high enough for self-phase modulation to take place is needed, but ideally not much higher than this. The reason for this is that at higher intensities more white light beams or channels will be created which in turn result in interference. Another risk with high intensities is that the glass can break down at the focal point of the beam, this results in a section of glass that can not be used anymore to generate white light. To manage the intensity Neutral Density (ND) filters are used for rough adjustments of the intensity and a continuous optical attenuator is used for the fine adjustments. The second parameter is the numerical aperture of the beam, for the generation of white light there is an ideal aperture, which is best found through adjustment in the setup. To vary the numerical aperture an aperture is present in the WLG setup. The last important parameter for the generation of white light is where the light is focused into the bulk glass slab. This is adjusted by an translation stage on which the lens focusing the light is placed.

In figure 3.2 it can be seen that the white light exiting the window after WLG is diverging. For further use of this beam in the setup this is not wanted, therefore the light is collimated into a parallel beam again. This is done using a off-axis parabola, which in the figure is simplified to a positive lens as seen in the schematic drawing. As discussed in subsection 2.2.1 the light generated using WLG still contains a residual component of the 800 nm source beam. The intensity of this light is high compared to the supercontinuum, for this reason this component of the light should be filtered out. This is done using a short pass filter as seen in the figure 3.2. For the setup which is used for the TAS measurements the cut-off wavelength of this filter is 750 nm. This ultimately results in a white light spectrum as shown in figure 3.3. From this spectrum it can be seen that the range of absorption measurements is from about 450 nm to 750 nm for the current setup.

After walking through the whole setup in figure 3.2 there are still some things which are worth considering. The first is the bandwidth of this white spectrum generated by this setup, because the bigger bandwidth dispersion and the resulting chirp in the signal should be taken into consideration. Thus as few as possible optical components should be used after the WLG setup and with a as low as possible Group-Velocity Dispersion (GVD) and Group-Delay Dispersion (GDD). Besides this the WLG has a property that makes it ideal for femtosecond TAS measurements, this is that after the process of WLG the pulses still have a width of around 150 fs. Another property which is not used in this setup but is worth noting is that all the resulting light is in phase with each other and thus still coherent. This process does also not change the polarization direction of the light.

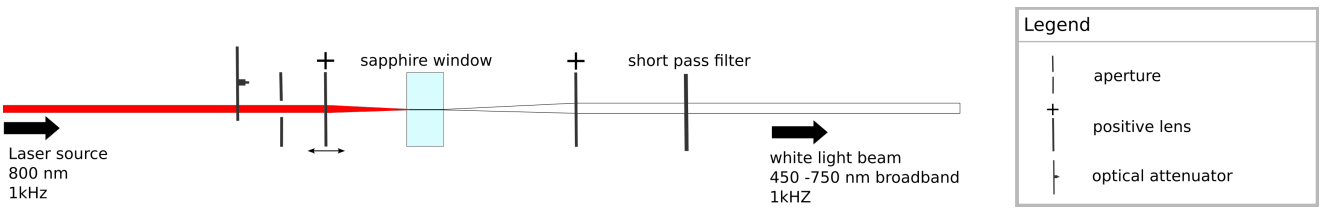

Figure 3.2: Schematic drawing of a White Light Generation (WLG) setup, like the one used to get a broadband spectrum for the probe beam.

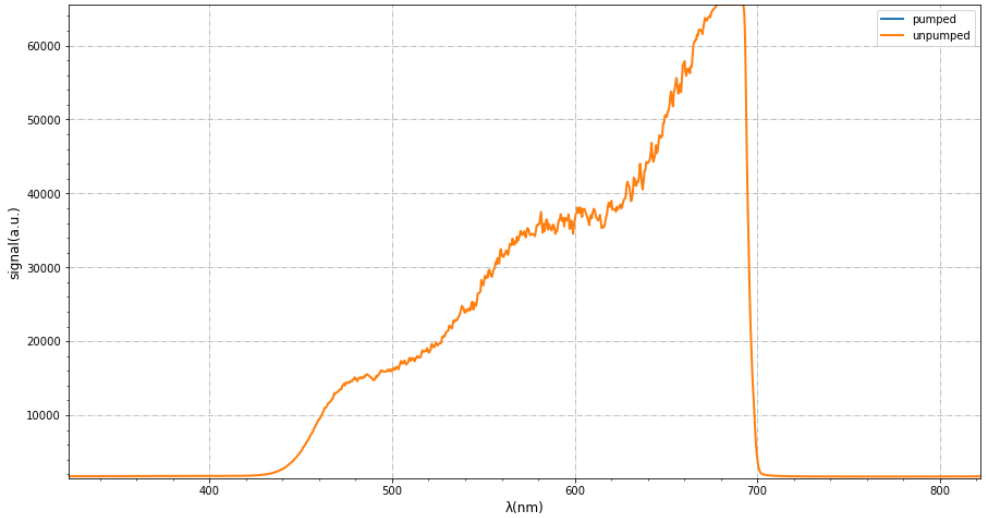

Figure 3.3: White light spectrum from the setup which is used for the probe beam.

3.1.3 Pump beam

The pump beam is used to excite the sample of which a femtosecond TAS measurement is taken. To do so in the most efficient way the wavelength of the beam should be tuned to a absorption wavelength of the sample. For the setup to be used with a wide range of samples it would be useful for the pump beam to have a adjustable wavelength, this can be achieved using a Noncollinear Optical Parametric Amplification (NOPA) setup. To keep the pulse short after passing the NOPA a pulse compressor is also implemented into the setup. The pump beam also needs to have an adjustable optical path length to choose a specific delay between the pump and the probe beam pulses, this is realised in the delay stage. Another requirement for the pump beam is that it repetition rate is half that of the probe beam, because later on measurements will be taken when the sample is not pumped as a reference. At first the NOPA setup will be considered, followed by the pulse compressor. After this the delay stage and the blocking of every other pulse will briefly be considered.

A NOPA is a setup where a specific spectral part of an broad spectrum is amplified. In depth information on the underlying working principles of the NOPA and Optical Parametric Amplification (OPA) processes can be read in the theory in subsection 2.2.2. For the setup it is most important that a NOPA can amplify a seed signal using a high photon energy pump beam. In figure 3.4 a schematic drawing is shown of a setup which does this. The first thing the incoming laser light passes through in this setup is a telescope. This telescope is used to decrease the beam diameter, this results in turn into a higher fluence of the beam. The higher fluence will prove to be useful in the amplification later on.

After this the beam is split to generate a white light beam and a pump beam with a higher photon energy. This last beam contains about 95% of the power of the beam split by the beamsplitter. To give the beam a higher photon energy the process of Second Harmonic Generation (SHG) is used, this process is discussed in depth in the theory in subsection 2.2.2. For an optimal conversion into the second harmonic the phase matching of the light is optimised using a half wave plate which can be rotated. Following this SHG takes place in the Barium Borate (BBO) crystal, after which the residual incident light is filtered out using a short pass filter. For the other beam a setup similar to the one seen with the probe beam is used, this results in a broadband white light beam.

Both the white light beam and SHG beams are focused into another BBO crystal, which amplifies the seed beam as seen in figure 3.4. For this specific setup the white light beam is the seed and will be amplified and the SHG is the pump beam. The seed and the pump beam are set up to be at specific angle from each other and the crystal is aligned so that critical phase matching occurs. This results that the setup can be used with a wide range of different wavelengths. The selection of the wavelengths which is amplified comes from the temporal overlap of the pump and the seed beam in the BBO crystal. Because the pump beam is much shorter(50 fs) than the white light seed(150 fs) the pump beam limits the bandwidth of the amplified spectrum. For adjusting this overlap and selecting a center wavelength the upper-right mirror in figure 3.4 is mounted on a translation stage to change the optical path length of the SHG beam. If the power of the amplified seed still is not sufficient, another NOPA setup could be added in series to get a higher beam power.

One of the downsides of a setup as seen in 3.4 is that it results in relatively long pulses in the range of 150 fs. The reason for this is chirp which is induced to the pulses in this setup. This chirp can be corrected for in a prism pulse compressor, this is a setup consisting of two prisms which induces a negative GDD. The result from this negative GDD is that it compensates the positive GDD which is induced by the setup before it, resulting in less chirp in the exiting light. From this decrease in chirp also in turn results a shorter pulse length as seen

before in subsection 2.1.3 in the theory. In figure 3.5 the geometry and components this setup consist of is shown. The negative GDD in this setup is achieved by dispersing the light so that different wavelengths travel a different optical path length. This ideally results in a negative chirp which is equal to the positive counterpart of the light which is being compressed. The GDD induced by this setup mainly depends on the distance between the tips of the prisms.[8]

After leaving the prism compressor, the beam is sent through the delay stage as seen in figure 3.1. This part of the setup is used to vary the optical path length of the pump beam, this is needed to let pulses from the pump and probe to arrive at the same time or at a specific delay. For the temporal evolution of processes to be measured this is essential. The optical part of this part the delay stage is quite simple it consist of a retro-reflector which is mounted on a motorized linear translation stage. The retro reflector consist of three mirrors all perpendicular to each other, this results in the reflected light beam always being parallel to the incoming light beam. The position of the retro reflector can be specified to a resolution of 0,1 μm using the motorized translation stage. To convert the difference in path length to a difference in delay equation 3.1 can be used. In this equation c is the speed of light and l is the path length in meters and t the time it takes to travel this length in seconds. For convenience and further reference some conversions using equation 3.1 are shown in table 1, in this table a value of 300.000.000 $\frac{m}{s}$ is used to make it more convenient than using the exact number. This is justified since this table should only be used for rough approximations and references.

$$c = \frac{l}{t} \tag{3.1}$$

time	pathlength	path	time
1 ns	30 cm	1 m	3,33 ns
100 ps	3 cm	10 cm	333 ps
10 ps	3 mm	1 cm	33,3 ps
1 ps	300 μm	1 mm	3,33 ps
100 fs	30 μm	100 μm	333 fs
10 fs	3 μm	10 μm	33,3 fs

Table 1: The path length light travels in an given amount of time on the left and the inverse on the right, both are in the range between 1 ns and 10 fs.

When the light has passed the delay stage the only thing that is left to do is to halve the repetition rate of the beam. This is done by blocking every other laser pulse by an optical chopper. For this chopper to work properly it is directly triggered by a signal from the laser light source. The frequency of the chopper is set to 500 Hz and a phase is selected so the laser beam is not clipped by the optical chopper. After this only every other beam will pass through the chopper and continue its path to the sample. This results in the probe switching between arriving at the sample in its ground state or its excited state.

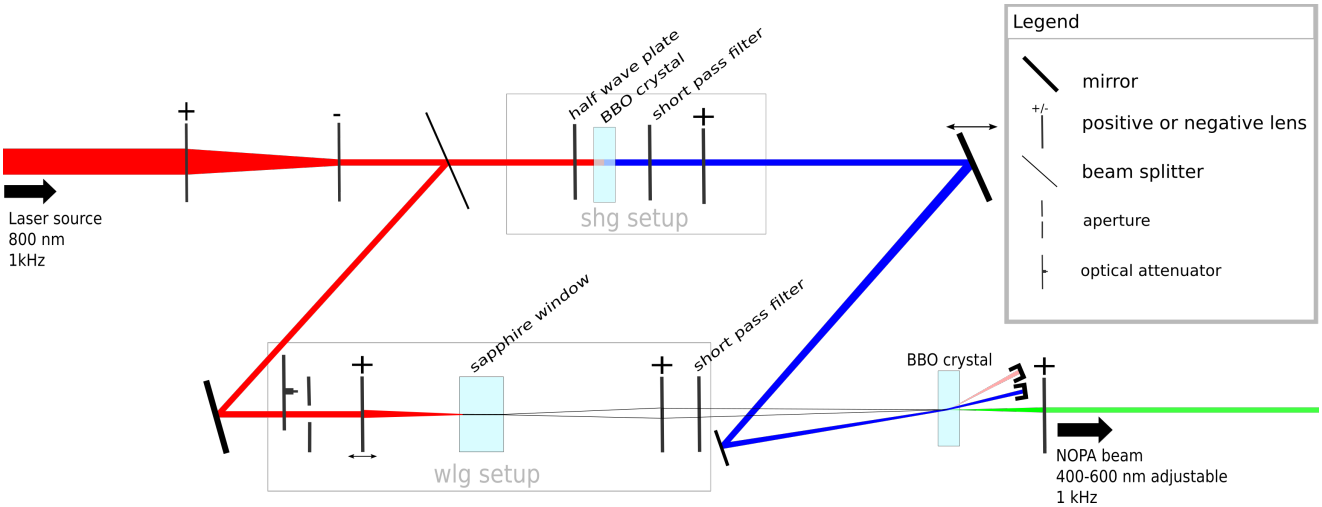

Figure 3.4: Schematic drawing of the Noncolinear Optical Parametric Amplification (NOPA) setup which is part of the setup for the pump beam.

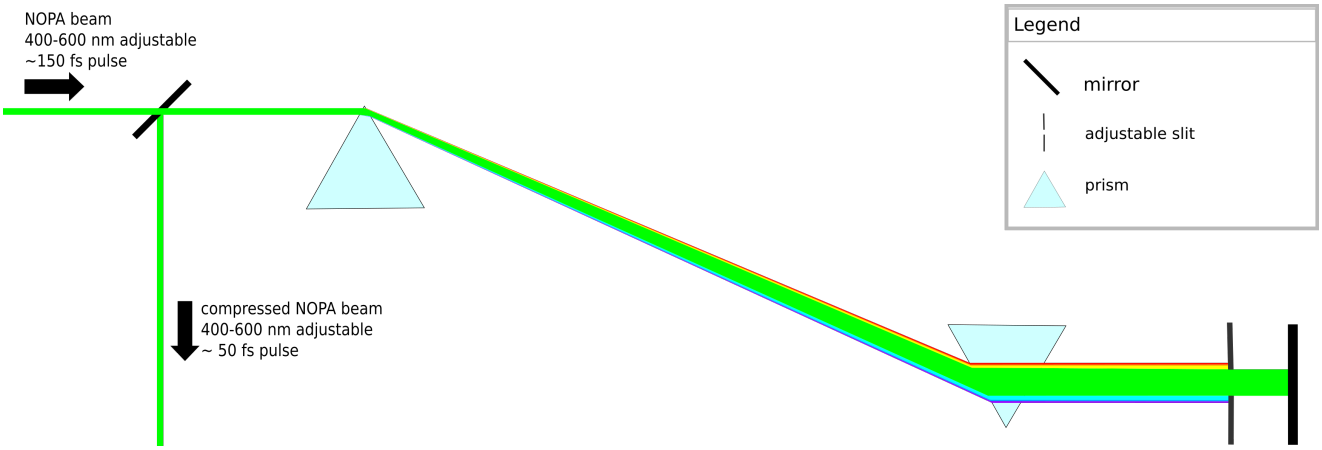

Figure 3.5: Schematic drawing of the prism compressor, which is used to compress the pulses after passing the Noncolinear Optical Parametric Amplification (NOPA) stage in the setup.

3.1.4 Interaction with the sample

In figure 3.1 there can be seen that the pump and the probe beam cross at a sample. For performing TAS measurements the pump and the probe beam are aligned to cross at a small angle from each other at this point. The pump and the probe beam are both focused in this point by lenses. For the pump beam a lens with a bigger focal length is used resulting in the pump beam being bigger in its focal point than the probe beam. This assumes that the two beams have a similar size before focusing. Because of this a sample placed in the beams has a bigger area which is pumped then will be probed. This is done to ensure pumped species are in the probed area.

Behind the focal point and in line with probe beam a lens is placed to generate a one to one image of the sample plane into an optical fibre. This is done by placing the fibre and the sample both at two times the focal length of the lens used for this. The light from the probe beam is sent into the fibre to a spectrometer to turn the light into a measurable spectrum. The pump beam will also be picked up by a mirror besides the lens to measure if the sample has been pumped or the pump beam has been blocked by the chopper using a photodiode. This can all be seen in figure 3.1.

3.1.5 Spectrometer

The last part of the optical setup is the spectroscope, a schematic drawing of the spectroscope setup is shown in figure 3.6. This device separates the spectral components spatially to be measured by a line camera. The light coming into the spectrometer comes from a optical fibre as mentioned before. This light first passes through a slit which can be considered as a new point source for the spectrometer setup. The diverging light from this slit is in turn collimated and redirected by a curved mirror. This light is sent to a diffraction grating, which disperses the light at a different angle depending on the wavelength of the light. After this this dispersed light is focused onto a line camera to detect the resulting spectrum. Most of the intensity of the light dispersed by the grating is in the first order, but in some cases higher orders can also be detected. If the spectral width of the measured light is broader than one octave higher orders can also be observed. This is not the case for the current TAS setup since the white light has a narrower spectral band than one octave.

The grating used in the spectrometer, has a high line spacing or low amount of lines per distance. Because of this a broad spectral range can be measured, but at the cost of spectral resolution. Fortunately this loss in spectral resolution is not that significant, since the pulses and processes are so short their spectra are relatively broad. More in depth information on diffraction and gratings can be found in Appendix B.

The spectrometer in combination with a line camera has been characterised for a specific wavelength range from 323 nm to 822 nm. This range is sufficiently wide to cover the whole visible range where measurements will be executed. For measurements in a lower wavelength region another region has been characterised, this range spans from 129 nm to 616 nm. The wavelength calibration of the camera in combination with the spectrometer has also been part of this project. For this report this range is not used since the white light and thus the region of which the absorbtion can be measured only spans from about 450 nm to 750 nm as seen in figure 3.3.

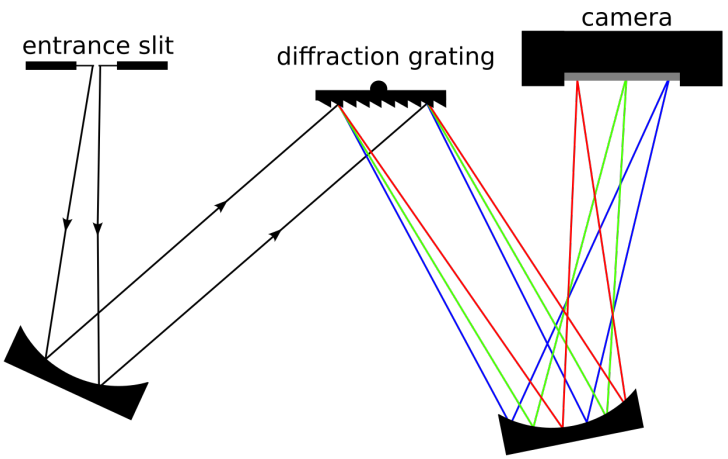

Figure 3.6: Schematic drawing of the optical setup of the spectrometer which is used to measure the spectrum of the probe beam.

3.2 Data-acquisition

In this section will be described how the result from the a TAS measurement are acquired and processed to a final dataset. First the interaction at the position of the sample which the setup aims to measure is considered. Following this a description of a single measurement of the line camera and photodiode will be given and at last a a full measurement cycle is described.

When taking TAS measurements two types of situations can be considered: the pumped and unpumped one. First the unpumped will be looked at. In this situation the pump pulse is blocked by the optical chopper and thus only the probe pulse reaches the sample. This situation is the same as a static absorption spectrum, which means that the light entering the fibre only consist of the light of the probe pulse which is transmitted through the sample in its ground state. The reason for measuring this spectra is to acquire a reference to compare the pumped measurements to. This spectra is further referenced as the unpumped spectrum, reference spectrum or $I_0(\lambda)$. In the other situation both the pump and probe pulse arrive at the sample in this order respectively with a known delay between them. The sample will first interact with the pump pulse, which excites the sample from its ground state to a higher energy state. A know time after this the probe pulse will arrive at the sample and some the light from this pulse will pas through the sample and be focused into the fibre as seen before. The spectrum of the light entering the fibre in this situation can be used to compute the absorption of the excited state. This spectrum is in this case is called the pumped spectrum or $I^*(\lambda, \Delta t)$. From the spectra $I_0(\lambda)$ and $I^*(\lambda, \Delta t)$ the difference in absorption or optical density can be calculated. In equation 3.2 the formula which is used to do this is shown, note that this equation is the same as equation 2.2 but with other notations for the intensities.

$$\Delta OD(\lambda, \Delta t) = -log\left(\frac{I^*(\lambda, \Delta t)}{I_0(\lambda)}\right) \tag{3.2}$$

These different spectra will be captured using a line camera. During this project this camera has been integrated into the existing server infrastructure in the lab for easy control during automated experiments. The specific model of line camera which has been used is a Synertronic Designs Linescan-I-Gen2 Line. This camera is specifically designed to operate at a high sample rate of 10 kHz and with the short pulses the TAS setup is based on. The camera has a resolution of 1024 pixels, which after comparing to a calibration source through the spectrometer correspond to a specific wavelength. For doing measurements of the spectra of the probe pulse this camera is triggered by the laser source with a specific delay added. The integration time is variable but fixed for most measurements at 500 μs, this means that the integration window will always catch a single pulse. As mentioned before this camera measures the spectrum of the probe beam every pulse. This results that ever 1 ms a spectrum can be captured due to the 1 kHz repetition rate of the laser source. Since for TAS pumped spectra and unpumped spectra are taken in alternating order, these spectra need to be distinguished from each other. This is done using the photodiode in the pump beam as seen in figure 3.1 and a corresponding digitizer from Synertronic Designs. The digitizer and the camera are synced to each other and measure at the same time, so the photodiode can measure if the sample is pumped or not. So for every single spectrum the camera will return the spectrum and if the photodiode was triggered or not.

For convenience one measurement consist of multiple spectra which will be sorted and averaged before returning a result. So when doing a measurement the user specifies the amount of spectra (between 2 and 50.000) and get in return two spectra. One of these spectra is the average spectrum of all the pumped spectra and one with the average of all unpumped spectra. With these spectra in turn the difference in absorption can be calculated using equation 3.2 as seen before. Ideally the absorption is calculated from the averaged pumped and unpumped spectra over as many pulses as possible to get a high signal to noise ratio. Given that the change in absorption is measured over a couple thousand pulses (which is a couple of seconds of measurement time) it is possible to observe changes of around 10^3 ΔOD with relative ease. For longer measurements for which is averaged over a lot more pulses significantly smaller changes in ΔOD could be measured.

To get from a single absorption spectrum to a time resolved spectrum another step is needed. This step is varying the delay by moving the delay stage. For convenience this process is automated using a python script which has been written during this project. This python script sets the stage to a position does a measurement and moves to the next delay step. Until all the specified delay steps are measured this protocol will repeat itself. This results in a dataset with three dimension which are as follows: wavelength, delay, change in absorption. For some measurements it makes more sense to do many short measurements over time at specific delays. This would for example be useful if a sample is suspected to degrade over time. In this case the protocol described before will still be the same, but can it be repeated for a set number of cycles. The results from every cycle can be averaged given that the amount of spectra per measurement stays constant.

4 Results

The first results which will be looked at are measurement of the coherent artifact in ethanol. These measurements will be considered first since they contain useful information about some important properties of the setup such as the temporal resolution of the measurements and the chirp in the measured spectra. After this measurements of rhodamine 6G dissolved in ethanol will be looked at, these measurements will be the first observations of processes with a real temporal evolution. If successful these measurements would prove the setup is in working order and more complex measurements on organics crystals could be proceeded with.

4.1 Coherent artifact in ethanol

The first measurement which have been execute is a measurement of the coherent artifact in ethanol. This artefact is an nonlinear effect between the pump and the probe beam, which is a combination of various nonlinear, nonresonant wave mixing processes between the pump and the probe pulse. For these processes to occur the two pulses need to be in the sample at the same time, therefore temporal overlap is a requirement for this process. Therefore this measurement is a great way of determining at what delay the two beams temporally overlap. This delay where the beams overlap in time is called time zero for further reference.

Since there were no measurements done before this the position of the delay stage corresponding to time zero was still unknown. Because of this first a rough measurement of the delay between the two beams was found using a photodiode and oscilloscope. This result in a position within accuracy of about 100 ps which corresponds to a range about 3 cm on the delay stage. This is a reasonable range to scan using Transient Absorption Spectroscopy (TAS).

Before moving on to these TAS first the spatial overlap of the two beams at the sample needs to be confirmed. This has been done using small apertures with sizes of 100 μm and 300 μm which can be placed at the positions of the sample for these measurements. These sizes in apertures where chosen since 100 μm is smaller than the beams at their focus and 300 μm a bit bigger than the beams. After the confirmation of this overlap the next step is finding the temporal overlap using a TAS measurement. Since the probe beam has a pulse width of around 150 fs steps in delay of 33 fs were chosen, which should result in the coherent artifact showing up in about 5 transient absorption measurements. This way the exact position of the translation stage was found for time zero. After this measurements with small delay steps of about 3 fs were taken of the coherent artefact in ethanol. For these measurements the pump beam has been adjusted to a centre wavelength of 530 nm.

In figure 4.1 the resulting TAS spectrum is shown. This kind of measurement with such small delay steps are only useful for characterising the setup, as later will be seen the temporal resolution of the setup is significantly higher than this step size of 3 fs.

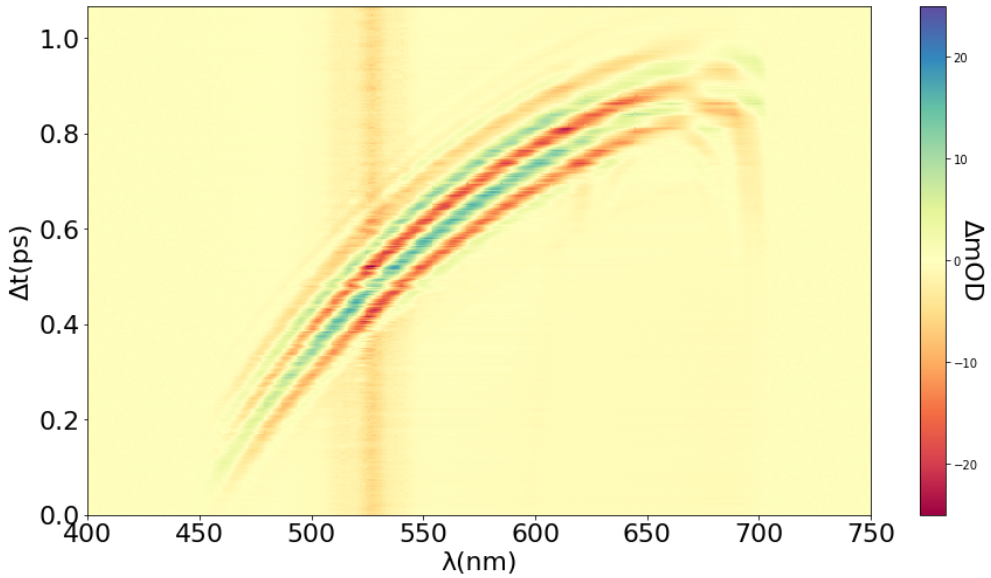

Figure 4.1: Transient Absorption Spectrum of ethanol, with the wavelength in nm on the x-axis ,the difference in delay from the start of the measurement in ps on the y-axis and the the difference in optical density indicated by color.

In figure 4.1 two different signals can be seen of which the coherent artifact is the most significant and prominent. The less significant signal is a constant background signal at 530 nm, this signal originates from the scattered light from the pump beam. For this reason this signal has the same spectral form as the pump beam and a negative value for ΔmOD. The coherent artifact is the oscillating signal through time when looking at a single wavelength. Due to this signal being a result of the temporal overlap of the pump and the probe beam, the signals length in time is limited by the shortest pulse. In this setup this is the pump pulse with a width of about 70 fs. Because the pump pulse is chirped and different wavelengths arrive at an offset time at the sample the signal of the coherent artifact is curved. This is caused by the dependence of the refractive index on the wavelength in dielectric media, in this case mainly the sapphire window in the setup contributes to this. From the data in figure 4.1 the resolution of the setup and the amount of delay induced by the chirp per wavelength can be derived.

The chirp of the TAS setup is defined by the curvature of the signal of the coherent artifact. For determining the chirp the central maxima in the coherent artefact has been taken. The foremost reason for this is that the signal of this maxima is consistently the highest value in the results and therefore easy to analyze. In figure 4.2 for every value of Δt the wavelength corresponding to the maxima value in that line is plotted. Through these data points a quadratic fit is applied, a quadratic fit is chosen since this resembles the characteristic of the chirp the best. By this quadratic fit the quadratic equation which is shown in equation 4.1 is determined. In this equation λ is the wavelength in nm and Δt_{chirp} the offset in time which result from chirp for a given wavelength in nm. The value of R^2 for this fit which has also been calculated and is equal to 0,99.

$$\Delta t_{chirp} = -1,24 \cdot 10^{-05} \cdot \lambda^2 + 5,37^{-02} \cdot \lambda - 5,37 \tag{4.1}$$

Now the curvature induced by chirp is known for this setup it could be corrected for. This would be done by shifting the delays for a wavelength depending on equation 4.1. Since the dynamics of the sample which will be discussed further in this report are relatively long lived this correction is not relevant at this point. For this reason the correction of the chirp will be implemented at a later time. Correction would be relevant when doing measurements of processes which require the maximum resolution of the setup this is especially crucial when integrating over a specific spectral area. When this is not needed a single wavelength can be considered in which case chirp correction is not needed. It should be noted in this case that time zero is at a different delay for each wavelength. In figure 4.2 also can be seen that the chirp of the probe pulse last approximately 800 fs.

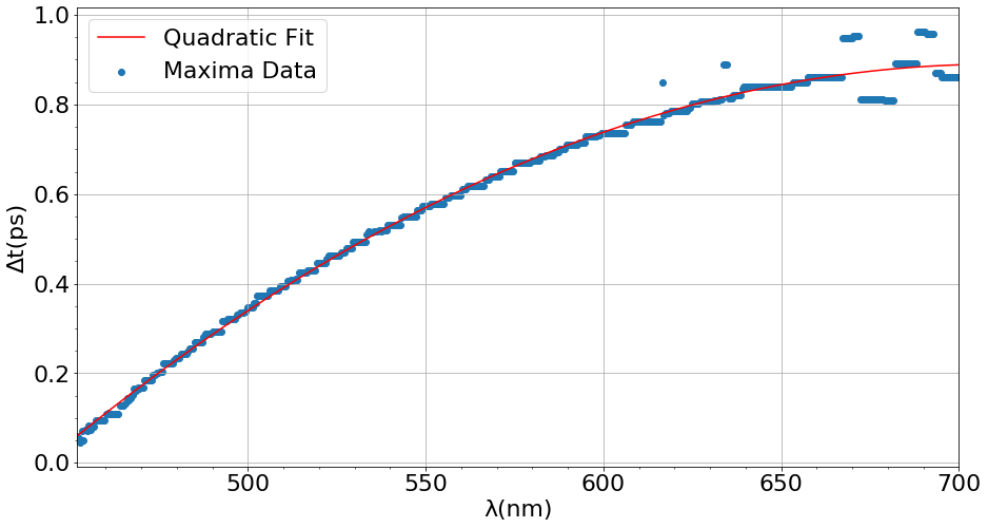

Figure 4.2: Maxima of the transient absorption spectrum of ethanol plotted with their wavelength in nm on the x-axis and their delay on the y-axis, through these data points a cubic fit is applied which is also shown in the plot. This data represents the offset in delay induced by chirp for a given wavelength.

From the data shown in figure 4.1 the maximum temporal resolution can also be determined. For now the temporal resolution will be considered as if the chirp has been corrected for by looking at a single wavelength. This is done since the curvature of the chirp is now known and can be corrected for. The resolution which interests us is thus the maximal possible resolution after correction for chirp.

In the measured coherent artefact the temporal resolution is equal to the amount of time the coherent artifact last when looked at a single wavelength. This results from the coherent artefact only being observed when the two pulses overlap in time as mentioned before. To analyze the duration of the coherent artefact the values of ΔmOD can be plotted against the delay Δt. This is exactly what is shown in figure 4.3 for a constant wavelength of 575 nm since at this wavelength the signal looks relatively strong and clean. When looking at this graph it can be seen that most of the signal encompasses a region consisting four peaks in ΔmOD above 10. This region is marked by two lines at the edge of the outermost peaks at 0,585 ps and 0,765 ps in figure 4.3. For now the 180 fs between these lines could be seen as the maximum reachable temporal resolution of the TAS setup after correction for chirp. This is only true for this specific configuration of the Noncollinear Optical Parametric Amplification (NOPA) setup for the pump beam, alongside with how well it is compressed in the prism compressor. For the following measurements of rhodamine 6G this resolution should be sufficient, since the dynamics are expected to be much slower than this resolution

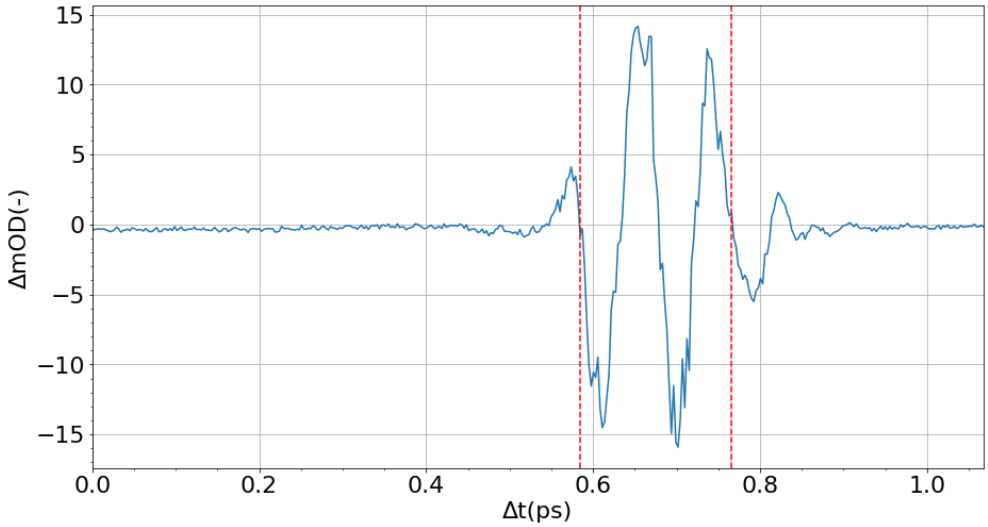

Figure 4.3: The difference in optical density plotted on the y-axis over the delay in ps on the x-axis at a constant wavelength of 575 nm for transient absorption in ethanol, with horizontal lines at 0,585 and 0,765 ps, these lines indicate how long the coherent artifact lasts.

4.2 Transient absorption in rhodamine 6G

After the measurements of the coherent artefact in ethanol, measurements of rhodamine 6G in ethanol were executed. For these measurements a flow cell was used with a pump to cycle the sample and get fresh species for every pulse. This makes sure that the samples are in their ground state before being excited and this prevents permanent bleach. The rhodamine 6G in ethanol solution which has been used in this flow cell was made to get an optical density at 530 nm between 0,5 and 1 in the flow cell with a path length of 200 μm, which is used during measurements. This translates to an optical density of 2,5 and 5 per mm which has been measured in a static absorption spectroscopy setup.

For the measurements shown in this section the pump beam has been adjusted to the absorption band at 530 nm of rhodamine 6G. First a measurement around time zero is taken to confirm that there is a difference in behavior between before and after time zero. The resulting TAS spectrum from this measurements is shown in figure 4.4. In this figure the same coherent artifact as in the measurements with ethanol can be seen, but this signal relatively weak in comparison to the other notable signals. Since the coherent artifact has already bean analysed in pure ethanol, no further thought is given to this in the measurement of rhodamine. Besides the coherent artifact two signals can be seen after time zero: a negative signal around 530 nm and a positive signal around 450 nm.

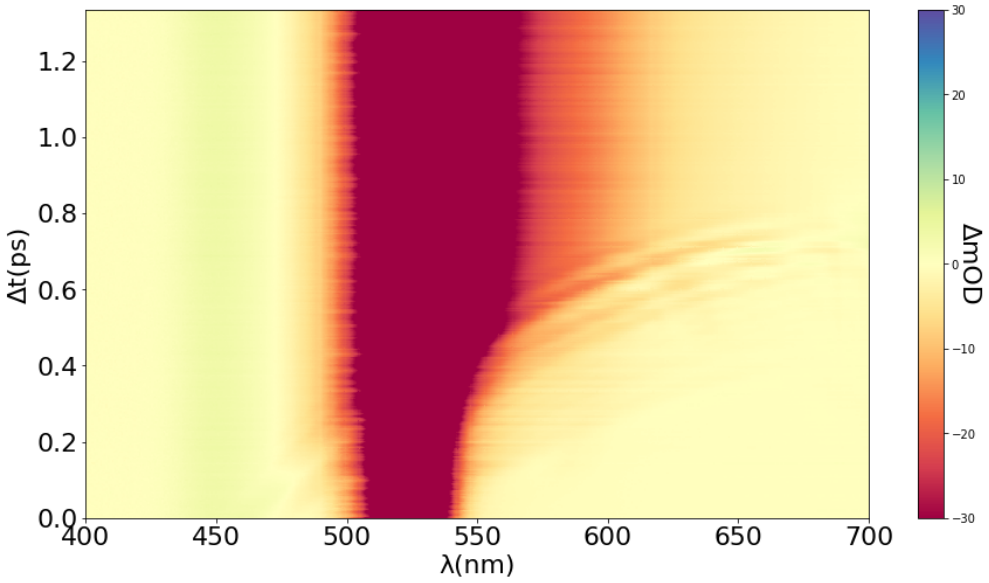

Figure 4.4: Transient Absorption Spectrum of rhodamine 6G dissolved in ethanol, with the wavelength in nm on the x-axis ,the difference in delay from the start of the measurement in ps on the y-axis, and the difference in optical density indicated by color, take note that negative values saturate this color scale.

These two signals are the first two ultrafast processes measured using the setup. The negative signal around 530 nm indicates that rhodamine 6G absorbs less light in its excited state than its ground state in this spectral region. When considering this is the same spectral region as the pump beam this signal is most certainly bleach of the ground state. The negative signal around 450 nm indicates that the excited state absorbs more light than the ground state. This in term corresponds to the physical process of excited state absorption. To get a better view of the spectral response of these signals the absorption spectrum at a delay of 1 ps is shown in figure 4.5. In this figure it can be seen that the signal with a maximum at 530 nm has the same spectral form as the pump beam, this makes sense if it would be a bleach signal. The other signal around 450 nm is much smaller than the bleach signal.

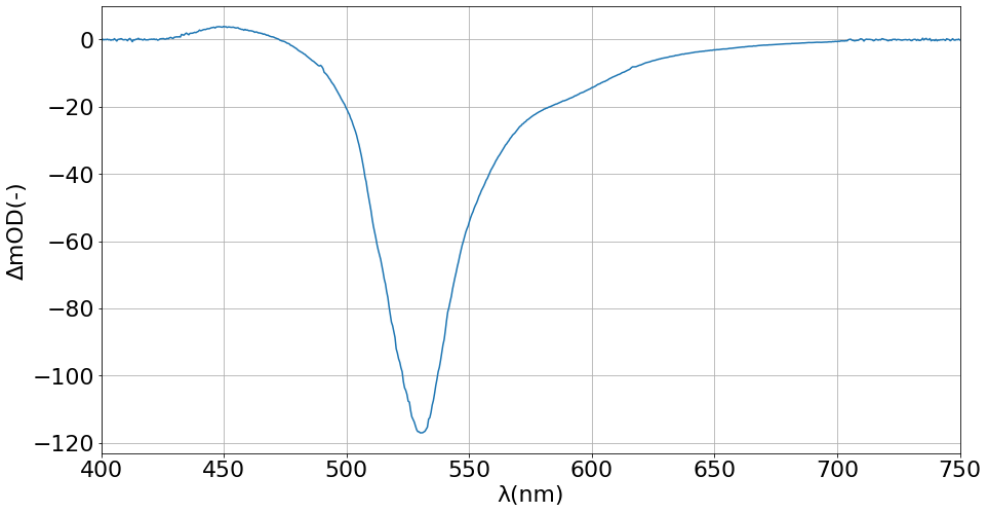

Figure 4.5: The difference in optical density plotted on the y-axis against the wavelength in nm on the x-axis at a constant delay of 1 ps for transient absorption in rhodamine 6G disolved in ethanol.

To analyze the temporal evolution of the behavior of rhodamine 6G it makes sense to do a longer measurement. In figure 4.6 a measurement with logarithmically spaced delay steps is shown. This measurement has an maximal delay of nearly 2 ns, which is the maximal delay which can be achieved with the current setup. This limit in delay arises from the maximum travel of the delay stage which is about 30 cm, this corresponds to a difference in path length of 60 cm which is equal to a delay of 2 ns. In figure 4.6 it is already visible that both the excited state emission and the bleach signal decay. For further analysis first the decay of the bleach signal at 530 nm is considered.

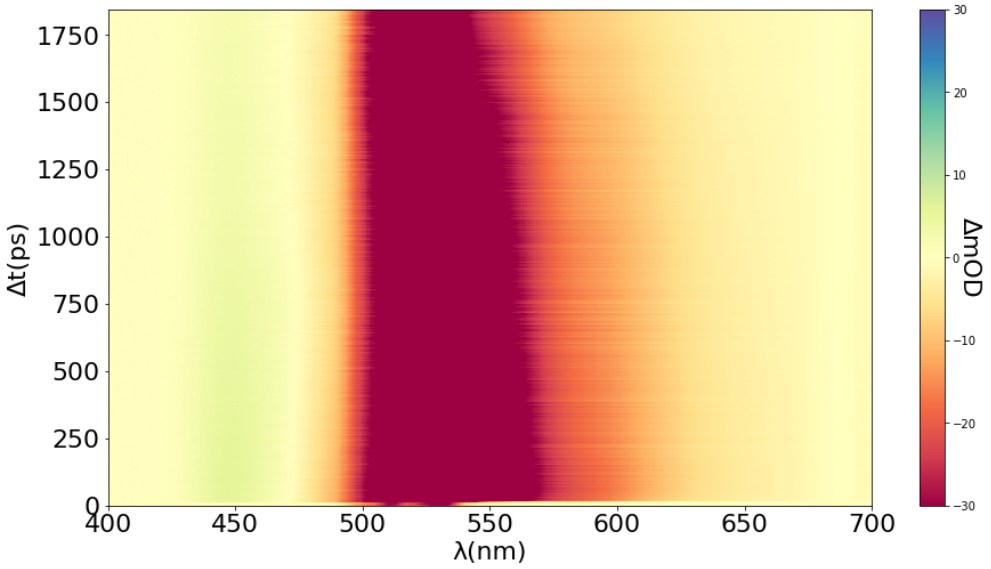

Figure 4.6: Transient Absorption Spectrum of rhodamine 6G dissolved in ethanol, with the wavelength in nm on the x-axis ,the difference in delay from the start of the measurement in ps on the y-axis with a logarithmic scale, and the the difference in optical density indicated by color, take note that negative values saturate this color scale. The range in delay for this measurement ranges from time zero to the maximal possible delay of 2 ns.

In figure 4.7a a line out of the decay of the bleach signal at 530 nm signal is shown. For this line out over time only the peak wavelength is plotted since chirp has not yet been corrected for. When this decay is considered it can be seen that it seems similar to a exponential decay right after time zero, after this a process with a longer lifetime seems to become relevant, which can't be properly viewed in the current range. To find the rate of decay in this initial period after time zero the data between 8,5 ps and 180 ps is plotted in figure 4.7b with a exponential fit applied to it. This exponential fit results in the exponential function shown in equation 4.2, this function has a decay constant of 18,8 ps. The value of R^2 for the executed fit was found to be 0,79.

$$\Delta mOD = -23,7 * e^{-\frac{1}{18,8}t} - 82,9 \tag{4.2}$$

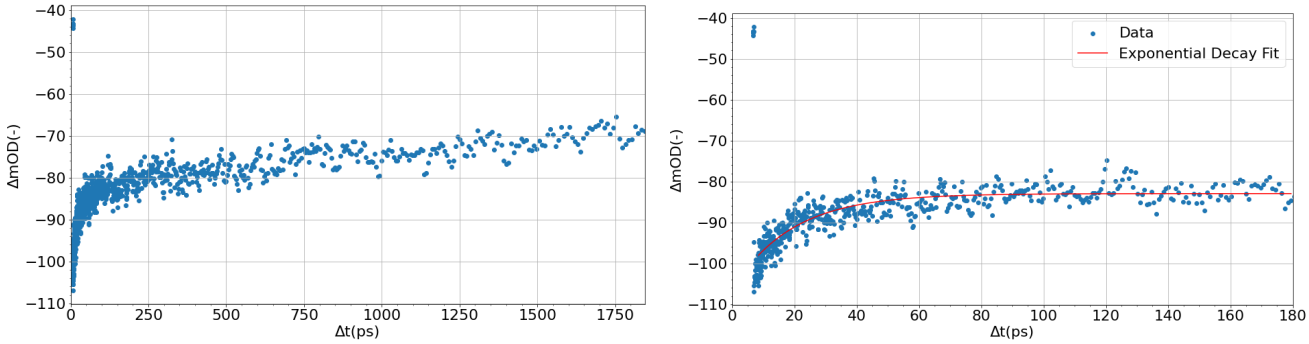

(a) Decay of the bleach signal over the full 2 ns delay range of the setup

(b) Decay of the bleach signal up to 180 ps with an exponential fit applied.

Figure 4.7: Decay from the measured bleach signal at 530 nm over time, with the full range on the left and a range up to 180 ps with an exponential decay curve fitted to it on the right.

In figure 4.8a a line out view of the excited state absorption signal at 450 nm is shown. This decay seems of a similar form as the decay of the bleach signal before this, which is a initial exponential decay followed by a longer process. To find the rate of this initial decay the data between 10 ps and 180 ps is plotted in figure 4.7b with a exponential fit applied to it. This fit results in an exponential function with a decay constant of 47,9 ps. The full equation for the applied fit is shown in equation 4.3, for this fit a value of R^2 equal to 0,97.

$$\Delta mOD = 1,99 * e^{-\frac{1}{47,9}t} + 2,43 \tag{4.3}$$

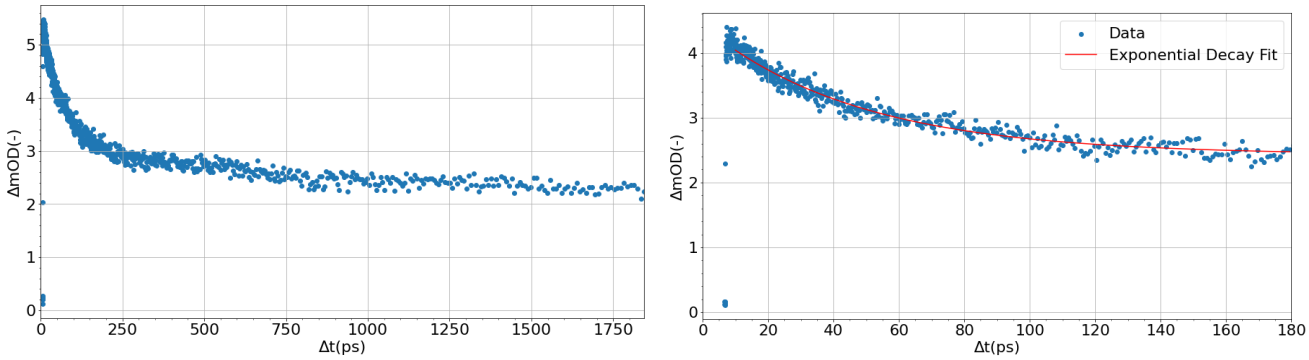

(a) Decay of the excited state absorption signal over the full 2 ns delay range of the setup.

(b) Decay of the excited state absorption signal up to 180 ps with an exponential fit applied.

Figure 4.8: Decay from the measured excited state absorption signal at 450 nm over time, with the full range on the left and a range up to 180 ps with an exponential decay curve fitted to it on the right.

5 Discussion

In this chapter the accuracy and the applicability of the results discussed in this report will be considered

First the coherent artefact measurements in ethanol are discussed. These results give insight in the limitation and behavior of the setup. The first result arising from these measurements is the chirp of the Transient Absorption Spectroscopy (TAS) setup, this is the dependence of the position of time zero on the wavelength. This chirp has been fitted to a quadratic function with a value of R^2 of 0,992 from this can be assumed that the chosen fit seems reasonable. The quadratic function shown in equation 4.1 can be used to correct for the chirp by shifting the delay for time zero. When the chirp is not corrected for this results in an offset in the delay, from the lowest to the highest wavelength this offset is about 800 fs. For measurements were integrating over a specific spectral region is required the chirp needs to be corrected to reach the maximum temporal resolution of the setup.

From the same data the maximum temporal resolution can be found. This is the resolution when the result has been corrected for chirp or when looking at a single wavelength. The value for this was found to be approximately 180 fs. This value is duration of the coherent artefact when viewing a single wavelength. The value of 180 fs seems relatively high since the pump pulses after leaving the prism compressor normally would have widths of 50 to 70 fs. This has routinely been confirmed using auto-correlation measurements and other research proves similar setups were able to reach resolution similar to the width of the pump pulses in their TAS setups.[9] Luckily this does not affect the result in rhodamine 6G, since the processes in this sample are not so short lived to require the maximum resolution.

When the results so far are considered these seem in line with existing literature. For the measurements of rhodamine 6G a bleach signal at 530 nm is found and a excited state absorption signal at 450 nm. This is similar to the response of rhodamine 6G in other TAS studies, in other studies besides this behavior also excited state absorption in the range from 450 nm till 700 nm with a long lasting dynamics around 530 nm is visible. It makes sense that this behavior is not seen in the results discussed here since for these studies the sample was pumped at a different wavelength. In the results shown in this report these dynamics are covered by the signals of the bleach in the pumped spectral region. These dynamics can also be measured using this setup but for this the pump beam should be adjusted to excite the sample at lower wavelengths.[10]

When the decay dynamics of the bleach signal at 530 nm are considered this seems to be dominantly exponential at first and after that a slower process takes over. This slower process could not be measured by the current TAS setup since it lives for much longer than the maximum delay of 2 ns, which can be scanned by the setup. To the initial decay from 8,5 to 180 ps an exponential fit was applied, this resulted in a decay constant of 18,8 ps and the full function shown in equation 4.2. The value of R^2 for the fit of this function is equal to 0,79 which is quite low. Since an exponential decay seems reasonable from an physical point of view and when the curve is viewed in figure 4.7b it seems to follow the data, it can therefore be seen as an adequate description of the process. For determining the behavior of the long lived decay there is not enough data at this point.

When the decay dynamics of the excited state emission signal at 450 nm are considered these seem to be a similar form as the bleach signal. This result again looks like an initial exponential decay followed by a longer process which can not be properly seen in the 2 ns delay window. To analyze the initial decay from 10 to 180 ps a exponential fit was applied which resulted in a decay constant of 47,9 ps and the full function shown in equation 4.3. The value of R^2 for the fit of this function is equal to 0,97 which is already a lot better than value for the bleach fit. For similar reason as mentioned with the bleach signal this fit will be seen as an adequate result for now.

6 Conclusion

During this project a Transient Absorption Spectroscopy (TAS) setup has been developed to measure the temporal evolution of excited state absorption in organic crystals with a temporal resolution around 100 femtoseconds. While this report focuses on the first measurements using this setup the development of the line camera control software, experimental control software and the building and development of this setup were also a big part of this project as a whole and essential to arrive at the final goal of the project. The eventual goal of this project was to characterize the main limitations of the developed TAS setup and validate the setup through the means of measurements on a sample with ultrafast excited state processes. This is done to prepare this setup for measurements on less documented samples and organic crystals with more intricate behavior. The goal of this project has been reached through two types of measurements: TAS measurements in ethanol to characterize the limitations of the setup and measurements in rhodamine 6G dissolved in ethanol to validate the setup by analyzing a first sample with excited state dynamics.

The measurements in ethanol were successful in determining the chirp in the setup and defining a approximate temporal resolution for the current setup. The chirp of the setup originates form the broad spectrum of the probe pulse(450-700 nm) due to dispersion of this pulse it is spread out temporally. This results in the shorter pump pulse scanning through the longer probe pulse resulting in a curvature between the delay depending on the wavelength. The extra delay induced by the chirp was determined to be of a quadratic form. The specific quadratic relation between the offset in delay depending on the wavelength can be concluded to be $\Delta t_{chirp} = -1,24 \cdot 10^{-05} \cdot \lambda^2 + 5,37^{-02} \cdot \lambda - 5,37$. This characteristic curve results from the current configuration of the probe beam and is thus only applicable in the current setup in the corresponding spectral range for the probe beam. Using this determined curve results will be corrected for the chirp in the future. The difference in delay induced by the lowest and highest wavelengths of the probe spectrum is about 800 fs. This delay is roughly equal to the pulse width of the probe pulses arriving at the sample in the current TAS setup.

For determining the maximal temporal resolution no rigorous definition has been made yet, but still a rough estimate can be made about this value. The value found for the maximal temporal resolution of the current TAS setup is 180 fs. This value is relatively high compared to the expected resolution, but the cause for this has not been determined yet. From comparable setups it is known a temporal resolution between 40 and 70 fs should be reachable. It is notable that maximal temporal resolution is heavily depends on the pulse width of the pump pulses, for this reason adjustments in the setup of the pump beam can directly influence this. Since rhodamine 6G does not have ultra short dynamics in the range of our resolution, this value is not relevant for these measurements.

For the measurements in rhodamine 6G two significant signals were found: the bleach signal around 530 nm in the pumped spectral region and an excited state absorption signal around 450 nm. These signals are in line with other literature, which seems to validate that the TAS setup is in working order. When the initial decays of these signals upto 180 ps are considered the bleach decays exponentially at a decay rate of 18,8 ps and the excited state absorption signal decays exponentially at a rate of 47,9 ps. After this for both processes a much slower decay starts which could not be properly viewed using the maximum delay of the TAS setup of 2 ns. For these decays no literature was found, but the fact that the decay of processes is seen adds to the validity of the developed TAS setup.

So summarizing this the following conclusions can be made:

- The femtosecond TAS setup has an well defined quadratic chirp which is now known and can be corrected for in the spectral region of the probe beam.
- The current setup presently has a maximum temporal resolution of roughly 180 fs on the condition that a single wavelength is analysed or the chirp has been corrected for.
- The executed measurements on rhodamine 6G are in line with expectations and seem to confirm the validity of the developed setup.

All of this proves very promising for future use of the developed setup.

7 Outlook

As read in the conclusion the developed Transient Absorption Spectroscopy (TAS) setup proves to be working like desired and is able to measure the temporal evolution of excited state dynamics of molecules with a temporal resolution about 180 femtoseconds with success. This opens the possibility for the spectroscopic research of excited state dynamics of organic crystals. Therefore this will also be the first next step in continuing research using the developed TAS setup. As part of this project there already have been attempts to do TAS measurements on organic crystals, but with no results so far.

Besides this the current setup has been build separate from the final setup which will combine TAS and Ultrafast Electron Diffraction (UED). For this reason the next step will be integrating a replica of the current setup into this combined setup. This would give rise to the possibility to do TAS and UED experiments at temperatures around 10 K and in vacuum right after each other as mentioned in the introduction. The software, knowledge and procedures which were developed during this project can easily be transferred to this undertaking.

Besides this outlook on further research and applications using the developed TAS setup, there are also some recommendation to be made to improve the current setup. The first would be further developing the processing software to easily correct the results for chirp. This would give the possibility of integrating over a spectral range with results measured near the temporal resolution. By doing this the noise can possibly be reduced without needing extra measurement time.

Another recommendation would be finding the cause for the higher than expected maximal temporal resolution for the setup. When this is found it could be minimized or eliminated increasing the resolution. This should be possible since literature shows resolutions between 50 to 70 fs for similar setups.

Besides this the current analysis software could be expanded upon to give more options for processing and analyzing results. Especially more development should be done in determining the statistical significance and confidence bounds of determined values. Another function which would be useful to implement would be analysis of the drift of the results over time during a measurement. But besides adding these statistics and analysis of drift over time new functions should be added as needed for more complex TAS measurements.

8 Literature

[1] D. Giancoli, *Physics for scientists & engineers with modern physics*. Pearson, 2014.

[2] H. Schwoerer, *Fourier transformation for experimental physicist*, 2013.

[3] A. Brodeur and S. Chin, "Ultrafast white-light continuum generation and self-focusing in transparent condensed media," *JOSA B*, vol. 16, no. 4, pp. 637–650, 1999.

[4] T. Imran and G. Figueira, "Intensity–phase characterization of white-light continuum generated in sapphire by 280 fs laser pulses at 1053 nm," *Journal of Optics*, vol. 14, no. 3, p. 035 201, 2012.

[5] A. Dharmadhikari, F. Rajgara, and D. Mathur, "Systematic study of highly efficient white light generation in transparent materials using intense femtosecond laser pulses," *Applied Physics B*, vol. 80, pp. 61–66, 2005.

[6] E. Kelleher, M. Erkintalo, and J. Travers, "Fission of solitons in continuous-wave supercontinuum," *Optics Letters*, vol. 37, no. 24, pp. 5217–5219, 2012.

[7] P. Atkins, *Physical Chemistry*. Oxford University Press, 2014.

[8] G. Taucher and H. Schwoerer, *Optical path length in prism compressor*, 2013.

[9] U. Megerle, I. Pugliesi, C. Schriever, C. F. Sailer, and E. Riedle, "Sub-50 fs broadband absorption spectroscopy with tunable excitation: Putting the analysis of ultrafast molecular dynamics on solid ground," *Applied Physics B*, vol. 96, pp. 215–231, 2009.

[10] F. Brandl, S. Bergwinkl, C. Allacher, and B. Dick, "Consecutive photoinduced electron transfer (conpet): The mechanism of the photocatalyst rhodamine 6g," *Chemistry–A European Journal*, vol. 26, no. 35, pp. 7946–7954, 2020.

[11] K. Riley, M. Hobson, and S.J.Bence, *Mathematical methods for physics and engineering*. Cambridge University Press, 2020.

[12] D. Jordan, *Mathematical Techniques*. Oxford University Press, 2010.

[13] E. Hecht, *Optics*. Pearson, 2017.

A Fourier transform and auto-correlation

The Fourier Transformation proves as a quite useful tool when considering some optical phenomena. This is not that weird considering it transforms functions into a form which describes the frequencies present in the original function and light consist of electromagnetic waves. In this section first the Fourier Transform itself is looked at, after which some examples are shown which prove to be useful.

Before looking at Fourier transformations it is useful to look at the Fourier series. This series is used to describe any periodic function in terms of sin and cosine components. The reason for doing this is to make it easier to analyse the function, because sinusoidal functions are well understood and their integration repeats in simple patterns. A Fourier series for any periodic signal can be written as shown in equation A.1. And the coefficients for this equation can be found in the equations A.2, A.3 and A.4

$$s(x) = A_0 + \sum_{n=1}^{\infty} \left(A_n \cos\left(\frac{2\pi n x}{T}\right) + B_n \sin\left(\frac{2\pi n x}{T}\right)\right) \tag{A.1}$$

$$A_0 = \frac{1}{T}\int_{-\frac{T}{2}}^{\frac{T}{2}} s(x)dx \tag{A.2}$$

$$A_n = \int_{-\frac{T}{2}}^{\frac{T}{2}} s(x)\cos\left(\frac{2\pi n x}{T}\right)dx \quad \text{and} \quad n \geq 1 \tag{A.3}$$

$$B_n = \int_{-\frac{T}{2}}^{\frac{T}{2}} s(x)\sin\left(\frac{2\pi n x}{T}\right)dx \quad \text{and} \quad n \geq 1 \tag{A.4}$$

The problem with the Fourier series is that it can only be used with periodic functions. Because optical pulses and some other optical processes are non periodic, another approach is needed to define them in sinusoidal functions. This can be done using the Fourier transform, this transformation is analogous to the Fourier series in equation A.1 but integrates the function over over the infinite domain R instead of only one period. The resulting transformation is shown in equation A.5.

$$f(\omega) = \int_{-\infty}^{\infty} \hat{f}(t)e^{i2\pi\omega t}dt \tag{A.5}$$

Before moving on to the description of optics using Fourier transformations the transformation of a Gaussian function is considered. The reason for this is the relevance of this function to laser light sources an some interesting properties of this function. In equation A.6 the standard form of this equation is shown.

$$Ce^{-at^2} \quad \text{and} \quad C = \sqrt{\frac{a}{\pi}} \tag{A.6}$$

When the Fourier transform is used on a formula in the form of equation A.6 it results in another Gaussian function, but depending on the variable ω. The standard deviation of these two Gaussian curves are $\sigma_x = \frac{1}{\sqrt{2a}}$ and σ_ω. This results in $\sigma_x \cdot \sigma_\omega = 1$, which shows that if the original Gaussian is broad it transform is narrow and vise versa. The dependence on each other of these two functions is analogous to the Heisenberg uncertainty principle which is observed in quantum mechanics.[11][12]

A.1 Auto-correlation

Auto-correlation is the correlation of a signal with a delayed copy of itself as a function with a specific delay. This correlation between two signal proves to be useful when measuring the pulse width of a laser pulses. The signal of an Auto-correlation signal is defined as a function $f(t)$ multiplied by itself with a offset of δ.

To arrive at the shape of the original function the convolution of two function is needed. For auto-correlation these two functions are $f(t)$ and this same function with a offset δ. This convolution can be derived from the Fourier transform and is shown in equation A.7.

$$(f * f)(\delta) = \int_{-\infty}^{+\infty} f^*(t)f(t-\delta) \tag{A.7}$$

For most laser light sources the signal of a pulse can be considered Gaussian, this is also true for the pulses considered in this report. The function used to determine the pulse width of a single pulse in regards to the auto-correlation signal is shown in A.8. This Gaussian is representative of the form of the envelope of a laser pulse.

$$g(t) = e^{\left(-\frac{t^2}{\tau^2}\right)} \tag{A.8}$$

After solving the convolution with itself for this function the following equation shown in equation A.9 is found. As can be seen this function is again a Gaussian function.

$$(g * g)(\delta) = \tau\sqrt{\frac{\pi}{2}}e^{\left(-\frac{\delta^2}{2\tau^2}\right)} \tag{A.9}$$

For the use case considered in this report mainly the width of the original pulses and the width of the auto-correlation signal are important. When looking at the resulting width of the auto-correlation signal in equation A.9, there can be seen that this is $\sqrt{2}\tau$. For the original function shown in equation A.8 the width is equal to τ, therefore the width of the auto-correlation signal can be converted by a factor $\sqrt{2}$ In equation A.10 the formula for this conversion is shown.

$$\sigma_{g*g} = \sqrt{2}\sigma_g \tag{A.10}$$

B Diffraction

Diffraction is an essential part to the spectrometer setup which has been explained in chapter 3, but is also the base for the UED experiments which can be executed in the complete setup as read in section 1. This section only focuses on the diffraction of light by optical gratings, since this is relevant to the setup and the data acquired from the TAS measurements. As said in chapter 1 no understanding of UED is needed for this report and therefore it will not be considered.

But what is the phenomenon of diffraction exactly? Francesco Grimaldi one of the first people doing detailed research on diffraction of light called the phenomenon as follows; "The effect is a general characteristic of wave phenomena occurring when part of a wavefront, be it sound, a matter wave, or light, in some way." and this is still true today. This phenomenon of diffraction is really not different from regular interference only has it become customary to talk of diffraction when considering a large number of waves. There are two types of diffraction which are Fraunhofer and Fresnel Diffraction, these are also known as near-field and far-field diffraction. Since for the purpose of this report only the far-field diffraction is relevant only Fresnel Diffraction is further considered.

The specific case of diffraction which is of interest for this report is diffraction between multiple slits wich is also called an optical grating. This kind of diffraction is well known and documented in optics, after some derivations a intensity profile can be calculated for this kind of diffraction. In equation B.1 the formula for this intensity profile is shown. This formula consist of a product of two parts these two parts originate from to processes which give rise to diffraction with multiple slits. The first which is noted on the left of the formula is interference for a single slit and the second on the right is interference between multiple light beams. In equation B.1 $I(\theta)$ is the intensity of the light after passing the grating for a given angle, θ the angle of the light after passing the slit , λ is the wavelength of the light passing through the slit, b is the width of the slits, N the amount of slits the light passes trough and s the separation between the slits. When the Intensity $I(\theta)$ is plotted as a result of varying θ this results in the intensity pattern shown in figure B.1. In this figure it can be seen that the pattern is similar to interference between multiple beams, but in an envelope function which is the single slit interference pattern.

$$I(\theta) = I_0\left(\frac{sin\left(\frac{\pi}{\lambda}bsin(\theta)\right)}{\frac{\pi}{\lambda}bsin(\theta)}\right)^2\left(\frac{sin\left(\frac{N\pi}{\lambda}d\sin(\theta)\right)}{sin\left(\frac{\pi}{\lambda}dsin(\theta)\right)}\right)^2 \tag{B.1}$$

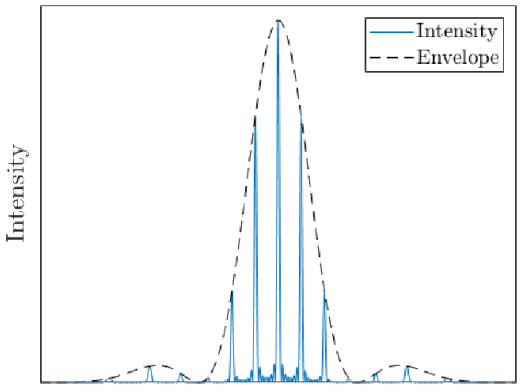

Figure B.1: Intensity pattern for interference between multiple slits

In most cases the main interest in the intensity profile shown above lies in the peaks which have relatively high intensities compared to the rest of the pattern. For these cases equation B.1 can be simplified to give the maxima

of the intensity profile. The resulting equation is shown in equation B.2 in which m indicates the order of the diffraction peak. This equation and the one shown before concerning diffraction are dependent on the wavelength. For this reason diffraction can be used to spatially divide different wavelengths. Spatially dividing wavelengths makes it suitable for spectroscopy, because the wavelength components do not overlap anymore an therefore their individual intensity can be measured.

$$d\sin(\theta) = m\lambda \tag{B.2}$$

Besides gratings consisting of slits, there are also some other kinds of gratings like transmission gratings and reflective gratings which can be used for spectroscopic purposes. Transmission gratings are made of translucent material with periodic grooves in them to bend the light passing through them and reflective grating work in a similar way but reflect the light. The ways of using diffraction for spectroscopic purposes so far have some big disadvantage. The first is that most the optical power ends up in the zeroth order, this light can not be used for spectroscopic purposes because all wavelengths overlap in this order. Another way power is lost is because the light is spread out over a number of low irradiance orders. To achieve a higher efficiency a reflective grating can be created with triangular grooves, this shifts energy out of the zeroth order. This kind of grating can be described using the equation B.3 or equation B.4 which is the same put written to give the angle of the maximum of the diffracted light. These gratings are widely used today and can be found in many spectroscope designs. One of the most important parameter for choosing a grating to use for spectroscopy is line spacing, which is the inverse of the amount of lines per unit of distance, which is often specified in specification sheets. When this spacing gets smaller the the diffraction pattern is spread out over a bigger distance, which creates a higher spectral resolution. This comes in return at the downside of having a smaller wavelength range and a lower intensity in comparison to a higher line spacing. Another characteristic of diffraction gratings is that the higher wavelengths of one order can overlap with low wavelengths of the next order. It has to be taken into account that this is a possibility and should especially be considered when taking spectroscopic measurements of high bandwidth light.[13]

$$d\left(\sin(\theta_i) - \sin(\theta_m)\right) = m\lambda \tag{B.3}$$

$$\theta_m = \arcsin\left(\sin(\theta_i) - \frac{m\lambda}{d}\right) \tag{B.4}$$